**Atmospheric
Chemistry
and Physics
Discussions**

N deposition in the tropics

I. Trebs et al.

Dry and wet deposition of inorganic nitrogen compounds to a tropical pasture site (Rondônia, Brazil)

I. Trebs[1], L. L. Lara[2], L. M. M. Zeri[3], L. V. Gatti[4], P. Artaxo[5], R. Dlugi[6], J. Slanina[7], M. O. Andreae[1], and F. X. Meixner[1]

[1]Max Planck Institute for Chemistry, Biogeochemistry Department, Mainz, Germany
[2]Centro de Energia Nuclear na Agricultura (CENA), Laboratorio de Ecologia Isotópica, Universidade de São Paulo, Piracicaba, São Paulo, SP, Brazil
[3]Max Planck Institute for Biogeochemistry, Jena, Germany
[4]Instituto de Pesquisas Energéticas e Nucleares, CQMA, Atmospheric Chemistry Laboratory, Cidade Universitaria, São Paulo, SP, Brazil
[5]Instituto de Física, Universidade de São Paulo (USP), São Paulo, SP, Brazil
[6]Working Group Atmospheric Processes (WAP), Munich, Germany
[7]University of Wageningen, Department of Environmental Sciences, Wageningen, AP, The Netherlands

Correspondence to: I. Trebs (ivonne@mpch-mainz.mpg.de)

Title Page	
Abstract	Introduction
Conclusions	References
Tables	Figures
◄◄	►►
◄	►
Back	Close
Full Screen / Esc	

Print Version

Interactive Discussion

EGU

EGU

Abstract

The input of nitrogen (N) to ecosystems has increased dramatically over the past decades. While total N deposition (wet + dry) has been extensively determined in temperate regions, only very few data sets exist about wet N deposition in tropical ecosystems, and moreover, experimental information about dry N deposition in tropical environments is lacking. In this study we estimate dry and wet deposition of inorganic N for a remote pasture site in the Amazon Basin based on in-situ measurements. The measurements covered the late dry (biomass burning) season, a transition period and the onset of the wet season (clean conditions) (12 September to 14 November 2002, LBA-SMOCC). Ammonia (NH_3), nitric acid (HNO_3), nitrous acid (HONO), nitrogen dioxide (NO_2), nitric oxide (NO), ozone (O_3), aerosol ammonium (NH_4^+) and aerosol nitrate (NO_3^-) were measured in real-time, accompanied by simultaneous (micro-)meteorological measurements. Dry deposition fluxes of NO_2 and HNO_3 are inferred using the "big leaf multiple resistance approach" and particle deposition fluxes are derived using an established empirical parameterization. Bi-directional surface-atmosphere exchange fluxes of NH_3 and HONO are estimated by applying a "canopy compensation point model". Dry and wet N deposition is dominated by NH_3 and NH_4^+, which is largely the consequence of biomass burning during the dry season. The grass surface appeared to have a strong potential for daytime NH_3 (re-)emission, owing to high canopy compensation points, which are related to high surface temperatures and to direct NH_3 emissions from cattle excreta. NO_2 also significantly accounted for dry N deposition, whereas HNO_3, HONO and N-containing aerosol species were only minor contributors. We estimated a total (dry + wet) N deposition of 7.3–9.8 kgN ha^{-1} yr^{-1} to the tropical pasture site, whereof 2–4.5 kgN ha^{-1} yr^{-1} are attributed to dry N deposition and ~5.3 kgN ha^{-1} yr^{-1} to wet N deposition. Our estimate exceeds total (wet + dry) N deposition to tropical ecosystems predicted by global chemistry and transport models by at least factor of two.

1. Introduction

The supply of reactive nitrogen (N) to global terrestrial ecosystems has doubled as a consequence of human activities, such as fertilizer application, cultivation of N fixing legumes and production of nitrogen oxides by fossil-fuel burning (Galloway, 1998). The deposition of atmospheric N species constitutes a major nutrient input to the biosphere. On a long-term scale, the increase of N inputs into terrestrial ecosystems may result in (i.) intensified trace gas exchange (ii.) enhanced leaching of nitrate and soil nutrients (e.g., K^+, Mg^{2+}, Ca^{2+}), (iii.) ecosystem eutrophication and acidification, (iv.) reduction in biodiversity, and (v.) increased carbon storage (Vitousek et al., 1997). Enhanced carbon storage due to N deposition has been shown to increase the terrestrial carbon sink in N-limited temperate ecosystems, which may have substantial impacts on global CO_2 concentrations (e.g., Townsend et al., 1996).

N deposition is considered to be relevant in the tropics due to widespread biomass burning activity and increasing fertilizer application. It was suggested by e.g., Matson et al. (1999) and Asner et al. (2001) that in contrast to temperate ecosystems, nitrogen-rich/phosphorus (P)-limited tropical rainforest soils may have a reduced productivity following excess N deposition, resulting in a decreased C-storage. Moreover, the humid tropical zone is a major source area for biogenic nitrous oxide (N_2O) and nitric oxide (NO) emissions from soils (Reiners et al., 2002). Enhanced N inputs to tropical forests are likely to increase nitrification/denitrification rates and, hence, the emission of NO and N_2O to the atmosphere (Hall and Matson, 1999). The conversion of tropical rainforest into cultivated land and pasture may lead to a sustained disturbance of the natural N cycle. During clearing and burning of tropical rainforest, biomass-associated N is volatilized and a large fraction is emitted in form of gaseous NH_3 (Trebs et al., 2004), which may result in considerable N losses of tropical ecosystems (Kauffman et al., 1998; Kauffman et al., 1995). This is affirmed by that fact that, in contrast to primary rain forests, plant growth in deforested areas is suggested to be limited by N rather than by P (Davidson et al., 2005; Oliveira et al., 2001).

EGU

N deposition in the tropics

I. Trebs et al.

EGU

The deposition of atmospheric N compounds occurs via dry and wet processes. Nitrogen dioxide (NO_2), ammonia (NH_3), nitric acid (HNO_3) and nitrous acid (HONO) are the most important contributors to dry N deposition. HNO_3 usually features a rapid downward (net deposition) flux to the surface (Huebert and Robert, 1985). By contrast,

5 the exchange of NO, NH_3, HONO and also NO_2 between surface and atmosphere may be bi-directional. The rates of production and consumption in vegetation elements and/or soils mainly determine whether net emission or net deposition of these species takes place. Turbulent diffusion controls the transport of gases and particles from the surface layer to the earth's surface. The uptake of trace gases by surfaces is con-

10 sidered to be dependent on physico-chemical and biological surface properties (Hicks et al., 1987), but also on the solubility and reactivity of the gaseous compound (Wesely, 1989). Hence, soil characteristics, plant stomata activity and trace gas chemical properties largely determine the deposition velocity. The atmospheric dry removal of aerosol particles, which may contain N species such as ammonium (NH_4^+) and nitrate

15 (NO_3^-), is a function of the particle size (Nicholson, 1988) but also depends on the particle density. Dry deposition is enhanced for large particles (especially those larger than a few micrometers) due to the additional influence of gravitational settling.

Wet N deposition is a result of in-cloud scavenging ("rainout") and below-cloud scavenging ("washout") of atmospheric N constituents (Meixner, 1994). The total (wet

20 + dry) N deposition ranges from 1–2 kgN ha^{-1} yr^{-1} for rural locations (e.g., North Canada) up to 30–70 kgN ha^{-1} yr^{-1} for urban N receptor regions (e.g., North Sea, European NW coast and NE U.S.) (Howarth et al., 1996). In contrast to moderately fluctuating air pollution levels that prevail in Europe, the United States and Asia throughout the year, tropical environments such as the Amazon Basin experience every year a

25 dramatic change from the "green ocean" clean background atmosphere to extremely polluted conditions during the biomass burning season. Only few studies exist were atmospheric wet N removal was determined experimentally in the tropics (Clark et al., 1998; Galloway et al., 1982; Likens et al., 1987; Srivastava and Ambasht, 1994). The chemical composition of precipitation in the Amazon region was determined in

previous studies by Andreae et al. (1990), Stallard and Edmond (1981), Lesack and Melack (1991) and Williams et al. (1997). Global chemistry and transport models (CTMs) such as MOGUNTIA have been applied to estimate total N deposition on a global scale (Holland et al., 1999). Model results suggest that net N deposition in the northern temperate latitude exceeds contemporary tropical N deposition by almost a factor of two. However, experimentally derived quantitative information about dry N deposition in tropical environments, required to validate these model predictions, has been lacking.

Kirkman et al. (2002) determined the surface-atmosphere exchange of NO, NO_2 and ozone (O_3) at a pasture site in the Amazon Basin (Rondônia, Brazil). In this paper, we complement their study by additionally estimating the surface-atmosphere exchange fluxes of NH_3, HNO_3, HONO, aerosol NO_3^- and NH_4^+ at the same pasture site. Our analysis is based on real-time measurements, supported by simultaneous measurements of (micro-) meteorological quantities covering the late dry (biomass burning) season, the transition period, and the onset of the wet season (clean conditions). Fluxes of NO_2, HNO_3, NH_3 and HONO are estimated by inferential methods. Wet N deposition was determined by collection of rainwater and subsequent analyses. We estimate the total (dry + wet) annual N deposition at this pasture site and the relative contribution of the individual N species.

2. Experimental

2.1. Field site

Measurements were performed during 12–23 September 2002 (dry season, biomass burning), 7–31 October 2002 (transition period) and 1–14 November 2002 (wet season, clean conditions) at a pasture site in the state of Rondônia, Brazil ("Fazenda Nossa Senhora Aparecida", FNS, 10°45′44″ S, 62°21′27″ W, 315 m a.s.l.). The site is located in the south-western part of the Amazon Basin. The location and a simplified sketch

of the measurement site are shown in Fig. 1. The primary rain forest at FNS was cleared by slash & burn activities in 1977. The vegetation at FNS is dominated by grass (*Brachiaria brizantha*) with small patches of *Brachiaria humidicola* and very few isolated palms and bushes, and the site is used as a cattle ranch (~200 "Blanco" cattle,

5 *Bos indicus hybrid*). FNS is located within a strip of cleared land about 4 km wide and several tens of kilometers long (Culf et al., 1996). The towns Ouro Preto do Oeste (~40 800 inhabitants) and Ji-Paraná (~110 000 inhabitants) are situated approximately 8 km and 40 km to the ENE and ESE of the site, respectively.

The instrumentation for trace gas/aerosol sampling and online analyses was ar-

10 ranged in an air conditioned wooden house. Rain samples were collected nearby the house (see Fig. 1). An automatic weather station (Met 1) was located in a distance of ~20 m to the S, and a meteorological tower (Met 2) was situated ~200 m to the NE of the inlets for trace gas and aerosol measurements. While the sampling site provides a sufficient uniform fetch expanding for 1–2 km from the sampling location in each direc-

15 tion (Andreae et al., 2002), local flow distortions may be caused by the wooden house and some instrument shelters. A more detailed description of the measurement site is given in Andreae et al. (2002) and Kirkman et al. (2002).

2.2. Sampling and analysis

Table 1 summarizes the specifications of the instruments for the measurement of trace

20 gases, aerosol species and (micro)-meteorological quantities. Water-soluble N containing trace gases (NH_3, HNO_3 and HONO) and related aerosol species (NH_4^+ and NO_3^-) were measured on-line. Air was taken from a height of 5.3 m above ground through a sophisticated inlet system, which was designed to reduce wall losses of soluble gases (especially HNO_3) and to minimize aerosol losses due to non-isokinetic

25 sampling (Trebs et al., 2004). Soluble gases were scavenged with a wet-annular denuder (WAD) (Wyers et al., 1993), which was combined with a Steam-Jet-Aerosol Collector (SJAC) (Khlystov et al., 1995) to collect particulate N species. For both gaseous and aerosol compounds, sample collection was followed by subsequent online anal-

ysis (ion chromatography (IC)) for anions and flow-injection analyses (FIA) for NH_4^+. Cycle times were set to 20 min (dry season), 40 min (transition period) and 60 min (wet season) (Trebs et al., 2004). Aerosol samples of either PM 2.5 ($D_p \leq 2.5\,\mu m$) or total suspended particulate matter (TSP) were collected. A detailed description and verifi-
5 cation of the measurement method and of the inlet system can be found in Slanina et al. (2001) and Trebs et al. (2004).

The chemiluminescence NO/NO_x analyzer (Thermo Environment Instruments) (see Table 1) was equipped with a molybdenum converter to transform ambient NO_2 to NO. However, the converter basically responds to the sum of NO_2 + HNO_3 + HONO + PAN
10 + aerosol NO_3^- + organic nitrates. Therefore, it is likely that NO_2 measurements might be biased by a positive artifact (Fehsenfeld et al., 1990). During our study, the inlet line for NO/NO_x measurements had a length of 25 m (inner diameter = 4.4 mm). Therefore, highly soluble and sticky species such as HNO_3 and HONO are assumed to be at least partly removed within the long inlet tubing. In addition, mixing ratios of HNO_3 and
15 HONO were usually below 0.5 ppb (Trebs et al., 2004), indicating that interferences would be marginal in case any of these gases would reach the chemiluminescence analyzer. PAN is a thermally unstable compound at temperatures even well below those observed at FNS (Kirkman et al., 2002) and aerosol NO_3^- was eliminated by the application of an inlet filter.
20 Also listed in Table 1 are those (micro)-meteorological sensors that were used to measure the quantities involved in this study, namely air temperature (T), relative humidity (RH), surface wetness, global radiation flux, momentum, latent and sensible heat flux and ingoing/outgoing short- and longwave radiation. Eddy covariance measurements were conducted using a Gill 3-D-sonic anemometer. The H_2O mixing ratio
25 was monitored by a fast LI-COR infrared gas analyzer, and its analog output was directly fed to the ultrasonic anemometer A/D converter. Post-processing of the eddy covariance data (EDDYWSC, software by Alterra, Wageningen University Research, Netherlands) resulted in 30 min averages of sensible heat flux, latent heat flux, friction velocity and Monin-Obukov length. More details on the eddy covariance measure-

N deposition in the tropics

I. Trebs et al.

ments and corresponding data evaluation/calibration procedures are given in Araujo et al. (2002).

Precipitation was sampled from 12 September to 14 November 2002 using a wet-only rainwater collector (Aerochem Metrics). A total of 23 rainstorm events were collected representing ∼100% of the precipitation in this period. Rain samples were stored in the dark at 4°C using polyethylene bottles which were previously rinsed with deionized water and preserved with Thymol. In order to trace possible contaminations, the sample pH was measured directly after sampling and before analysis. Analyses of NH_4^+, NO_3^- and NO_2^- were performed for all samples using a Dionex DX600 ion chromatograph at the Laboratório de Ecologia Isotópica, CENA/USP (São Paulo, Brazil). The detection limit was 0.05 μM for all species. More details about sampling and analysis procedures are provided by Lara et al. (2001).

Moreover, a twin Differential Mobility Particle Sizer (DMPS) was employed to measure the dry aerosol particle size distribution in the diameter range from 3 to 850 nm. The size distribution of particles with aerodynamic diameters from 1 to 4 μm was measured with an Aerodynamic Particle Sizer (APS) (Rissler et al., 2004; Vestin et al., 2005[1]).

3. Theory: estimation of dry and wet N deposition

3.1. Trace gas fluxes

Dry deposition fluxes of trace gases have been estimated using the inferential method, which is based on the "big leaf multiple resistance approach" (Wesely and Hicks, 1977; Hicks et al., 1987). The deposition flux (F) (μg m^{-2} s^{-1}) of a nonreactive trace gas for

---

[1] Vestin, A., Rissler, J., Swietlicki, E., and Frank, G.: Cloud nucleating properties of the Amazonian dry season biomass burning aerosol – measurements and modeling, in preparation, 2005.

which the surface is a sink under all ambient conditions is defined by:

$$F = -V_d \cdot X(z_{ref}) = -\frac{X(z_{ref})}{R_a + R_b + R_c} \tag{1}$$

where $X(z_{ref})$ is the trace gas concentration (μg m^{-3}) at the reference height z_{ref} (m) and V_d denotes the dry deposition velocity (m s^{-1}), which is the reciprocal of the sum of the turbulent resistance (R_a) (s m^{-1}), the quasi-laminar or viscous boundary layer resistance (R_b) (s m^{-1}), and the surface resistance (R_c) (s m^{-1}). According to Hicks et al. (1987) R_a between the reference height (z_{ref}) and the roughness length z_0 (m) is given by:

$$R_a = \frac{1}{\kappa \times u*} \left[\ln\left(\frac{z_{ref}}{z_0}\right) - \Psi_{H\left(\frac{z_{ref}}{L}\right)} \right] \tag{2}$$

where κ denotes the von Karman constant (0.41) and L is the Monin-Obukov length (m), a measure of atmospheric stability that is derived from the sensible heat flux and the friction velocity $u*$ (Garratt, 1992). $\Psi_H(z_{ref}/L)$ is the stability correction function for heat and inert tracers in its integral form (see Thom, 1975). The roughness length z_0 of the grass surface at the FNS site was taken as 0.11 m (cf. Kirkman et al., 2002) and z_{ref} was 5.3 m and 10 m for the WAD/SJAC and for the NO$_x$ measurements, respectively (Table 1). To account for conditions when the reliability of micrometeorological techniques was low, data were rejected for $u* \leq 0.01$ m s^{-1} and $z_{ref}/L \leq 5$, i.e. when extremely low turbulence and/or very high thermal stability was prevailing. Also, data were rejected for $z_{ref}/L \geq -5$, which reflects cases of very high thermal turbulence production (when Monin-Obukov similarity is no longer valid; Ammann, 1999).

R_b determines the exchange of gaseous matter by molecular-turbulent diffusion across the viscous laminar sublayer immediately above the vegetation elements and can be described by (Hicks et al., 1987):

$$R_b = \frac{2}{\kappa \times u*} \left(\frac{Sc}{Pr}\right)^{\frac{2}{3}} \tag{3}$$

N deposition in the tropics

I. Trebs et al.

EGU

where *Sc* and *Pr* are the Schmidt and Prandtl number, respectively. *Pr* is 0.72 and *Sc* is a strong function of the molecular diffusivity of the trace gas. Values for *Sc* were taken from Hicks et al. (1987) and Erisman et al. (1994) for the different trace gas species. The surface resistances R_c could not be directly determined from our field
5 measurements; hence values were adopted from the literature (see Sect. 4.4).

The inferential method is valid for trace gases whose mixing ratio at the soil and/or vegetation elements is zero. The observation of a net NO_2 deposition flux to the FNS pasture by Kirkman et al. (2002) justifies the application of the inferential model for NO_2 in our study. This is also valid for HNO_3, which typically features a rapid downward flux
10 with negligible R_c and corresponding high V_d (Hanson and Lindberg, 1991).

By contrast, NO, HONO and NH_3 may be both deposited to and emitted from surfaces. Formally, this can be accounted for by a so-called canopy compensation point concentration $X_c (\mu g\, m^{-3})$ (Hesterberg et al., 1996) that generally refers to the concentration of the compound just above the soil and/or vegetation elements (Nemitz et al.,
15 2004a):

$$F = \frac{X_c - X(z_{ref})}{Ra + R_b + R_c} \qquad (4)$$

The net NO emission from the FNS pasture site determined by Kirkman et al. (2002) was very low (0.65 ngN $m^{-2}\, s^{-1}$ or 0.17 kgN $ha^{-1}\, yr^{-1}$), thus we neglected any contribution of NO to the surface-atmosphere exchange of N species in our study. HONO is
20 generally assumed to be formed by heterogeneous reaction of NO_2 with surface water (Harrison et al., 1996) and it may subsequently be emitted from plant foliar cuticles or soil surfaces. Since there is no indication for any direct HONO emissions by plants (Schiemang et al., 2004), the HONO compensation point concentration X_c (HONO) is expected to be a function of the NO_2 mixing ratio (see Sect. 4.4).
25 To predict the bi-directional surface-atmosphere exchange of NH_3 at the FNS site, we applied a dynamic resistance model proposed by Sutton et al. (1998). Besides uptake and emission of NH_3 via plant stomata, the dynamic model accounts for absorption

of NH_3 by epicuticular water films under very humid conditions, and subsequent re-evaporation (capacitive leaf surface exchange). Since the FNS site is used as a cattle ranch and the NH_3 flux directly from the soil is assumed to be negligible compared to that originating from cattle excreta, we considered a direct NH_3 flux from cattle manure and urine $F(NH_3)_{excreta}$. The net NH_3 flux $F(NH_3)$ can be related directly to the NH_3 canopy compensation point concentration $X_c(NH_3)$ (Sutton et al., 1998) and is composed of its component fluxes through plant stomata, F_s (NH_3), the flux in or out of the epicuticular water film (adsorption capacitor), $F_d(NH_3)$, and $F(NH_3)_{excreta}$:

$$F(NH_3)_t = \underbrace{\frac{X_s(NH_3) - X_c(NH_3)}{R_s(NH_3)}}_{Fs(NH_3)} + \underbrace{\frac{X_d(NH_3)_t - X_c(NH_3)}{R_d(NH_3)}}_{Fd(NH_3)} + F(NH_3)_{excreta}$$

$$= \frac{X_c(NH_3) - X(NH_3, z_{ref})}{R_a + R_b} \tag{5}$$

where $X_s(NH_3)$ denotes the NH_3 stomata compensation point concentration ($\mu g\ m^{-3}$) and $R_s(NH_3)$ denotes the NH_3 stomata resistance (s m^{-1}). $X_d(NH_3)_t$ is the NH_3 adsorption concentration ($\mu g\ m^{-3}$) associated with the "leaf surface capacitor" at time step t and $R_d(NH_3)$ is the charging resistance of the capacitor (s m^{-1}) (see Sutton et al., 1998). $X_c(NH_3)$ is then determined by (Sutton et al., 1998):

$$X_c(NH_3)_t = \frac{X(NH_3, z_{ref})/(R_a + R_b) + X_s(NH_3)/R_s(NH_3) + X_d(NH_3)_t/R_d(NH_3) + F(NH_3)_{excreta}}{(R_a + R_b)^{-1} + R_s(NH_3)^{-1} + R_d(NH_3)^{-1}} \tag{6}$$

$X_s(NH_3)$ can be parameterized according to (Farquhar et al., 1980; Sutton et al., 1994):

$$X_s(NH_3) = \frac{161\,512}{T_S} \cdot 10^{(-4507.11/T(z_0))} \cdot \Gamma \cdot 17\,000 \tag{7}$$

where T_S is the surface temperature (K) which was derived from the outgoing longwave radiation by applying the Stefan-Boltzmann law. Γ is the ratio of apoplastic $[NH_4^+]/[H^+]$

EGU

and was adopted from the literature (Sect. 4.4). $R_s(NH_3)$ can be calculated from the measured latent heat flux LE (W m^{-2}) for relatively dry daytime conditions and in the absence of precipitation using the algorithm of Nemitz et al. (2004a). Furthermore, $X_d(NH_3)$ at time step t is a function of the adsorption charge and of the capacitance of the epicuticular water film (for details see Sutton et al., 1998). The values for the adsorption charge were adopted from Sutton et al. (1998) and the capacitance is a function of the epicuticular pH (see Sect. 4.4)

3.2. Aerosol fluxes

Up to date, no well established bulk resistance models exist for particle deposition. Significant discrepancies have been observed between experimental results and model predictions (Ruijgrok et al., 1995). The theoretical framework proposed by Slinn (1982) is widely used in modeling studies to predict particle deposition velocities. However, Wesely et al. (1985) derived an empirical parameterization for the dry deposition velocity V_p (m s^{-1}) of submicron sulfate aerosols ($D_p = 0.1–1.0\,\mu$m) to grass surfaces:

$$V_p = u* \cdot 0.002, \quad \text{for} \quad L \geq 0 \tag{8a}$$

$$V_p = u* \cdot 0.002 \cdot \left[1 + \left(\frac{-300}{L}\right)^{\frac{2}{3}}\right], \quad \text{for} \quad L < 0 \tag{8b}$$

This approach generally results in much higher V_p values for submicron particles than predicted by the Slinn model. Several other studies (Garland, 2001; Nemitz et al., 2004b; Vong et al., 2004) also showed that V_p to surfaces of low aerodynamic roughness may be much larger than predicted by the Slinn model, even for particles of different chemical composition than studied by Wesely et al. (1985). In this study, however, either PM 2.5 or TSP was sampled. NH_4^+ it is known to be largely attributed to fine mode aerosols with $D_p \leq 1.0\,\mu$m (Seinfeld and Pandis, 1998), which was also observed dur-

EGU

ing the SMOCC measurement campaign (Decesari et al., 2005[2]). By contrast, aerosol NO_3^- exhibited a bimodal size distribution (Falkovich et al., 2005). Since we did not find an empirical relationship in the literature to estimate V_p for aerosols with $D_p \geq 1.0\,\mu m$ and the contribution of coarse mode aerosol NO_3^- relative to that of fine mode aerosol NH_4^+ is presumably small (cf. Sect. 4.2, Table 2), the parameterization by Wesely et al. (1985) is considered as a reasonable approximation for both PM 2.5 and TSP samples.

3.3. Determination of characteristic time scales

The resistance-based approaches presented above to calculate surface-atmosphere exchange fluxes rely on the "constant flux layer assumption", which implies that the trace compounds considered are chemically-non-reactive tracers, such that their flux within the atmospheric surface layer is constant. However, sufficiently accurate fluxes of compounds that undergo rapid chemical transformation can be estimated as long as characteristic chemical time scales are one order of magnitude larger than turbulent transport times (Damköhler ratio $D_r < 0.1$) (De Arellano and Duynkerke, 1992). Following De Arellano and Duynkerke (1992) the characteristic time of turbulent transport τ_{turb} (s) can be calculated as:

$$\tau_{turb} = \kappa \cdot (z_{ref} + z_0) \cdot \left(\frac{\sigma_w^2}{u*}\right)^{-1} \qquad (9)$$

where σ_w denotes the standard deviation of the vertical wind component (m s^{-1}). Atmospheric stability strongly determines the time scale of turbulent transport, which

---

[2]Decesari, S., Fuzzi, S., Facchini, M. C., Maenhaut, W., Claeys, M., Rudich, Y., Artaxo, P., Guyon, P., Andreae, M. O., Mayol-Bracero, O. L., and Fisch, G.: Overview of the inorganic and organic composition of size-segregated aerosol in Rondonia, Brazil, from the biomass burning period to the onset of the wet season, in preparation, 2005.

N deposition in the tropics

I. Trebs et al.

EGU

typically ranges from a couple of seconds under unstable conditions up to 2.5 h under stable conditions (Dlugi, 1993).

For the characteristic chemical time scale of the NO-NO_2-O_3 triad, its photostationary equilibrium has to be considered. NO_2 is rapidly photolyzed to NO in the troposphere and it is formed back by reaction of NO with O_3. The overall chemical time scale of the NO-NO_2-O_3 triad τ(NO-NO_2-O_3) is given by the combination of τ(NO)=$(k_2 \times [O_3])^{-1}$, $\tau(NO_2) = k_1^{-1} = j(NO_2)^{-1}$ and $\tau(O_3) = (k_2 \times [NO])^{-1}$ (Lenschow, 1982) (where k is the reaction rate constant) and was calculated in accordance to Kirkman et al. (2002). Thereby, $j(NO_2)$ was estimated from global radiation data using a relation derived from simultaneous measurements of global radiation and $j(NO_2)$ in Amazonia during LBA-EUSTACH (cf. Kirkman et al., 2002).

HONO is rapidly photolyzed during daylight hours. The chemical time scale for daytime HONO photolysis is given by $\tau(HONO)_{photol.} = j(HONO)^{-1}$, whereby the parameterization provided by Kraus and Hofzumahaus (1998) was used to relate $j(HONO)$ to $j(NO_2)$. The chemical time scale of heterogeneous HONO formation at nighttime $\tau(HONO)_{het.}$ was derived by considering the HONO production rate P_{HONO} (ppb h^{-1}) determined directly from our measurements (see Sect. 4.3). Homogeneous daytime HONO formation may proceed via reaction of NO with OH radicals; however, this process is very slow and can be neglected compared to daytime HONO photolysis (Lammel and Cape, 1996).

Photochemical reactions involving NH_3 and HNO_3 are not considered to contribute to any flux divergence since their chemical time scale is much larger than the time scale of turbulent transport (Pandis et al., 1995). By contrast, time scales to achieve gas/aerosol equilibrium between gaseous NH_3, HNO_3 and particulate NH_4NO_3 may occur within the time frame of turbulent transport (few seconds for submicron particles) and have to be explicitly considered here (Dlugi, 1993; Meng and Seinfeld, 1996). As reported by Trebs et al. (2005), the measured concentration product of $NH_3 \times HNO_3$ was persistently below the theoretical equilibrium dissociation constant of the pure NH_3/HNO_3/NH_4NO_3 system during daytime (RH<90%), but approached the theoreti-

N deposition in the tropics

I. Trebs et al.

cal equilibrium value during nighttime (RH>90%). The desired equilibration time scale $\tau(\text{NH}_3\text{-HNO}_3\text{-NH}_4\text{NO}_3)$ can be estimated according to (Wexler and Seinfeld, 1992):

$$\tau(\text{NH}_3-\text{HNO}_3-\text{NH}_4\text{NO}_3)^{-1}=3\overline{D}\times\int\limits_0^\infty\frac{m(R_p)dR_p}{\left(1+\frac{\lambda}{\alpha+R_p}\right)\times R_p^2\times\rho_p} \tag{10}$$

whereby the measured aerosol number size distribution was related to the aerosol mass size distribution $m(R_p)dR_p$. R_p is the particle radius (m), $\overline{D}$ is the geometric mean of the diffusivity of semi-volatile gaseous species (m^2 s^{-1}), m is the water-soluble particle mass (kg m^{-3}), λ is the mean free path of air (6.51×10^{-8} m at 293.15 K), α denotes the accommodation coefficient (0.001<α<1) (Wexler and Seinfeld, 1990), and ρ_p is the particle density. A value of ρ_p=1.35±0.15 g cm^{-3} was used as determined by Reid and Hobbs (1998) for Amazonian biomass burning aerosols.

The comparison of τ_{turb} with $\tau(\text{NO-NO}_2\text{-O}_3)$, $\tau(\text{HONO})_{photol.}$, $\tau(\text{HONO})_{het.}$ and $\tau(\text{NH}_3\text{-HNO}_3-\text{NH}_4\text{NO}_3)$ allows to test whether reactive species can be treated as a passive tracer during their vertical transport within the surface layer (D_r<0.1) and, consequently, if the application of the "big leaf multiple resistance approach" and the "canopy compensation point model" are justifiable.

3.4. Wet N deposition

Storm size influences the chemical composition of the rainwater, in the sense that larger storms tend to be more dilute. This dependence demands the use of volume weighted means (VWM) for the calculation of monthly and annual concentration averages. For each rainwater solute, the concentrations measured in the sample were combined to create a VWM concentration for each collection date:

$$\text{VWM}_a=\frac{\sum_{i=1}^n c_{ai}\times v_i}{\sum v_i} \tag{11}$$

where c_{ai} is the concentration of species a in sample i, n is the number of samples and v_i is the volume of precipitation solution for sample i. The corresponding wet deposition rates for September, October and November were derived by summation of the VWM concentration determined for each precipitation event throughout the month, and
5 subsequent multiplication by the mean of rainfall in the respective month obtained from historical time series (see http://www.aneel.gov.br). The annual wet N deposition was derived in a similar way; for instance, the VWM concentration obtained during September was considered as representative of the entire dry season and then multiplied by the historical mean rainfall for the dry season. The same procedure was performed for
10 October and November representing transition period and wet season, respectively.

4. Results and discussion

In the following, the general patterns of our results will be shown as diel courses of the medians of measured and inferred quantities. Diel courses will be presented either for part of the dry season (biomass burning, 12–23 September) or, where the investigated
15 quantities are relatively independent of season, for the entire measurement campaign (12 September–14 November 2002). To derive surface-atmosphere exchange fluxes of N-containing compounds, (micro)-meteorological data and NO_x/O_3 data were synchronized to the time resolution of the WAD/SJAC system. The convention of negative downward fluxes (net deposition) and positive upward fluxes (net emission) has been
20 adopted.

4.1. Meteorological conditions

In the Amazon Basin, nighttime radiative cooling usually results in the formation of a shallow, decoupled nocturnal boundary layer of high thermodynamic stability characterized by very low wind speeds; while the development of a deepening, convectively
25 mixed layer starts with the heating of the surface in the morning (Nobre et al., 1996;

Fisch et al., 2004). Median nighttime wind speeds at FNS were low ($\leq 1\,\mathrm{m\,s^{-1}}$). By contrast, wind speeds were substantially higher during daytime, ranging from 2 to 3 m $\mathrm{s^{-1}}$. The 24-h average friction velocity (u_*) was $\sim 0.16\,\mathrm{m\,s^{-1}}$ and reached maxima of $\sim 0.4\,\mathrm{m\,s^{-1}}$ around noon. Differences of u_* between the dry season, the transition

5 period, and the wet season were marginal. As a consequence of high global radiation fluxes (500–900 $\mathrm{W\,m^{-2}}$, median) during daytime, ambient temperatures at the FNS site ranged between 30 and 36°C during sunlight hours, while nighttime temperatures were much lower (20–25°C). High relative humidities (*RHs*) were observed during nighttime (90–100%), while daytime *RH* values usually dropped to 40–50% during afternoon

10 hours. Local meteorology changed only marginally from the dry season to the wet season. Strong rain events ($\geq 30\,\mathrm{mm\,h^{-1}}$) occurred in the afternoon hours during the transition period and the wet season. A more detailed description of diel meteorological conditions can be found in Trebs et al. (2005).

4.2. Concentrations

15 Median diel variations of NO, NO_2, O_3, NH_3, HNO_3, HONO and the inorganic aerosol species NH_4^+ and NO_3^- are shown in Fig. 2a–h for 12 to 23 September (dry season, biomass burning). Table 2 summarizes ambient mixing ratios measured during the dry season (12–23 September), the transition period (7–31 October) and the wet season (1–14 November). A detailed discussion of seasonal and diel cycles observed for NH_3,

20 HNO_3, HONO and aerosol NH_4^+ and NO_3^- is given in Trebs et al. (2004, 2005).

Despite intensive biomass burning activity during the dry season, NO mixing ratios were very low (Fig. 2d). The sharp peak between 06:00 and 09:00 LT was most likely due to rapid photolysis of accumulated nighttime NO_2 shortly after sunrise, when O_3 mixing ratios were still too low to re-oxidize significant amounts of NO (see Fig. 2e,

25 f). NO_2 was the most abundant N-containing trace gas during all three seasons and reached an average mixing ratio of ~ 5 ppb during the dry season. NO_2 featured a pronounced diel cycle with nighttime mixing ratios two times higher than during daytime

N deposition in the tropics

I. Trebs et al.

EGU

(Fig. 2e). Apparently, NO_2 was accumulated in a shallow nocturnal boundary layer of high thermodynamic stability due to: (i.) the low water-solubility of NO_2 and consequently its low affinity to be taken up by epicuticular water films and (ii.) chemical production through reaction of NO with O_3 in the absence of NO_2 photolysis. Through the transition period until the wet season, NO_2 mixing ratios declined by a factor of four. O_3 mixing ratios exhibited a typical diel variation, which mirrors that of NO_2 (high values during daytime and lower values during the night (Fig. 2f)). This was mainly caused by (i.) photochemical daytime production, (ii.) convective mixing within the boundary layer and from the free troposphere during daytime and (iii.) dry deposition and reaction with NO in a thermally stable stratified nocturnal boundary layer.

4.3. Characteristic timescales

Characteristic turbulent time scales (τ_{turb}) have been calculated according to Eq. (9) for z_{ref}=10 m (NO_x/O_3 measurements) and for z_{ref}=5.3 m (WAD/SJAC measurements) (cf. Table 1). To calculate the characteristic time scale for heterogeneous nighttime HONO buildup ($\tau(HONO)_{het.}$) (Fig. 3a), only dry season nighttime HONO production rates (P_{HONO}) were considered. For the transition period and the wet season P_{HONO} could not be determined since the HONO diel variation was substantially reduced (cf. Trebs et al., 2004). In contrast to other studies (e.g., Alicke et al., 2003; Harrison and Kitto, 1994; Lammel and Cape, 1996), our measurements revealed a relatively small average value of P_{HONO}=0.04 ppb h^{-1}. Figure 3a shows that τ_{turb} was at least two orders of magnitude smaller than $\tau(HONO)_{photol.}$ and $\tau(HONO)_{het.}$, resulting in $D_r \ll 0.1$. Considering the chemical time scale of the NO-NO_2-O_3 triad $\tau(NO-NO_2-O_3)$ (Fig. 3a), largest D_r values are found between 17:00 LT and 20:00 LT, exceeding a value of 0.2 (z_{ref}=10 m). However, during all other periods D_r for the NO-NO_2-O_3 triad ranged between 0.05 and 0.1. Therefore, we conclude that the application of Eqs. (1) and (4) to calculate surface-atmosphere exchange fluxes of NO_2 and HONO are justified, since chemical transformations are too slow to affect the vertical constancy of turbulent fluxes.

Title Page

Abstract | Introduction

Conclusions | References

Tables | Figures

◄ | ►

◄ | ►

Back | Close

Full Screen / Esc

Print Version

Interactive Discussion

EGU

The estimation of the equilibration time scale $\tau(NH_3\text{-}NO_3\text{-}NH_4NO_3)$ was performed by integrating over the measured particle size distribution according to Eq. (10), whereby two different cases were considered. Case 1 is an upper estimate (Fig. 3b), using an accommodation coefficient $\alpha=0.1$ (Wexler and Seinfeld, 1992) and taking into account only the inorganic water-soluble aerosol fraction ($\leq20\%$ of PM_{tot}) (cf. Trebs et al., 2005). Case 2, the lower estimate (Fig. 3c), was calculated using $\alpha=1$ and considering also water-soluble organic carbon (WSOC). The total water-soluble fraction (organic and inorganic) accounted on average for ~60% of the total aerosol mass (Decesari et al., 2005[2]). As shown in Fig. 3b, c $\tau(NH_3\text{-}NO_3\text{-}NH_4NO_3)$ increased substantially from the dry season through the transition period to the wet season. This is obviously caused by much higher particle number concentrations measured during the dry season when biomass burning took place (Vestin et al., 2005[1]). For case 1 (upper estimate) (Fig. 3b), D_r for the $NH_3\text{-}NO_3\text{-}NH_4NO_3$ triad during the dry season ranges from 0.1 to 0.17 at nighttime and is smaller than 0.1 during the day. During the transition period and wet season, D_r for the $NH_3\text{-}NO_3\text{-}NH_4NO_3$ triad is always significantly smaller than 0.1 (Fig. 3b). However, for case 2 (lower estimate) (Fig. 3c) nighttime D_r substantially exceeds a critical value of 0.1 during the dry season and the transition period.

To verify the theoretically derived values, results from a laboratory study will be discussed briefly. Condensation and evaporation of NH_3 and HNO_3 to/from particles have been investigated under controlled laboratory conditions. Particles were collected during field campaigns in 1991 (Brunnemann et al., 1996; Seidl et al., 1996) and 1993/1994 in the eastern part of Germany (Melpitz). The chemical aerosol composition was dominated by $(NH_4)_2SO_4$, NaCl and soot and is comparable to that described in Brunnemann et al. (1996) and Seidl et al. (1996). More than 90% of the NH_4NO_3 mass was found in the accumulation mode ($D_p \leq 1\,\mu m$). Timescales $\tau(NH_3\text{-}HNO_3\text{-}NH_4NO_3)$ were calculated using the algorithm proposed by (i.) Kramm and Dlugi (1994) and (ii.) Meng and Seinfeld (1996), resulting in $\tau(NH_3\text{-}HNO_3\text{-}NH_4NO_3)=100\text{--}500\,s$ for fine mode particles and $\geq880\,s$ for coarse mode particles. These values are comparable to

N deposition in the tropics

I. Trebs et al.

Title Page

Abstract	Introduction
Conclusions	References
Tables	Figures

◀ | ▶︎

◀ | ▶

Back | Close

Full Screen / Esc

Print Version

Interactive Discussion

[EGU](#)

characteristic times reported by Harrison et al. (1990) and Meng and Seinfeld (1996) and are in strong favor of our case 1 (upper estimate, Fig. 3b), which implies that the equilibration time scale was always much larger than that of turbulent transport. Nevertheless, it should be noted that the influence of the large soluble organic aerosol fraction typical for the Amazon Basin (cf. Trebs et al., 2005) on gas/aerosol partitioning processes is not exactly known. Taking into account the potential role of WSOC in enhancing aerosol water uptake and subsequently the uptake of gaseous species, equilibration time scales may be equal or even faster than turbulent transport (cf. Fig. 3c).

4.4.   The inferential approach: discussion of input parameters

Some surface parameters required for the inferential method to estimate of surface-atmosphere exchange fluxes for trace gases (Eq. 1–7) could not be directly derived from the results of our field measurements. Thus, lower and upper scenarios were estimated, comprising a certain range of surface-atmosphere exchange fluxes. These scenarios were obtained by varying surface parameters over a selected range based on results obtained from studies in temperate latitudes. Note that for all parameters and quantities presented, values indicated as "low" and values indicated as "high" correspond to the resulting lower and upper flux estimates, respectively.

4.4.1.   Surface resistances $R_c(HNO_3)$, $R_c(HONO)$ and $R_c(NO_2)$:

$R_c(HNO_3)$ was found to be zero in many studies (Dollard et al., 1987; Huebert and Robert, 1985). Very recently, Nemitz et al. (2004a) showed that non-zero, however, relatively small $R_c(HNO_3)$ may exist (R_c=15–95 s m^{-1}). $R_c(HONO)$ is considered to be only slightly higher than that of HNO_3 (Wesely and Hicks, 2000). The ranges of $R_c(HNO_3)$ and $R_c(HONO)$ used to estimate lower and upper surface-atmosphere exchange fluxes are given in Table 3. The surface uptake of HNO_3 and HONO is considered to be enhanced by the presence of epicuticular water films under the humid conditions at the site (lower R_c values were chosen for nighttime). $R_c(NO_2)$ has al-

N deposition in the tropics

I. Trebs et al.

[EGU](#)

ready been determined previously at the FNS site by Kirkman et al. (2002), hence no flux scenario is calculated for NO_2 and median diel $R_c(NO_2)$ values are taken directly from Kirkman et al. (2002) ($R_c(NO_2)$=200–300 s m^{-1}).

4.4.2. Bulk surface resistance $R_c(NH_3)$:

$R_c(NH_3)$ is derived from the sum of the parallel resistances $R_s(NH_3)$ and $R_d(NH_3)$. $R_d(NH_3)$ is calculated in accordance to Sutton et al. (1998) which resulted in $R_d(NH_3)$ >1000 s m^{-1} (daytime) and $R_d(NH_3)$ ≤100 s m^{-1} (nighttime). Since $R_s(NH_3)$ is not known for *Brachiaria brizantha* grass species, we limited the range of $R_s(NH_3)$ by considering the diffusion of H_2O and O_3 through plant stomata. For the upper NH_3 flux estimate, $R_s(NH_3)$ is derived from the measured latent heat flux (*LE*) during daytime (10:00–18:00 LT) (see Sect. 3.1). The transfer of H_2O through plant stomata is considered as a very efficient process, representing an upper boundary for trace gas stomata exchange. By contrast, the transfer of O_3 through plant stomata is considered to be limited by the low solubility of O_3. Therefore, $R_c(O_3)$ determined by Kirkman et al. (2002) is assumed to be equal to the bulk surface resistance $R_c(NH_3)$ during daytime, and $R_s(NH_3)$ is calculated as $R_s(NH_3)^{-1} = R_c(O_3)^{-1} - R_d(NH_3)^{-1}$, whereby the different diffusivities of O_3 and NH_3 are taken into account. From 07:00 to 10:00 LT, when evaporation of epicuticular water films contributed to *LE*, $R_s(NH_3)$ derived from $R_c(O_3)$ is used for both the lower and the upper flux estimate. Since stomata are thought to be closed during nighttime, $R_s(NH_3)$ is set to 1000 s m^{-1} for nighttime periods.

4.4.3. Compensation point concentration $X_c(HONO)$:

Up to date, only two studies provide an estimate for $X_c(HONO)$ (Harrison and Kitto, 1994; Stutz et al., 2002). Here, the relationship $X_c(HONO)$=0.03·$X(NO_2, z_{ref})$ was used, which was found for grassland in the recent study by (Stutz et al., 2002). This corresponds on average to $X_c(HONO)$=85 ppt at the FNS site.

Title Page

Abstract | Introduction

Conclusions | References

Tables | Figures

◀◀ | ▶▶

◀ | ▶

Back | Close

Full Screen / Esc

Print Version

Interactive Discussion

EGU

4.4.4. Apoplastic $[NH_4^+]/[H^+]$ ratio Γ and epicuticular pH:

For Γ, we have chosen values of 100 (lower estimate) and 200 (higher estimate), which range at the lower end of data reported for grass in the literature (Loubet et al., 2002; Spindler et al., 2001; van Hove et al., 2002). This may be justified by the poor soil N status at FNS (Kirkman et al., 2002), because N absorbed by the root medium strongly affects the leaf tissue NH_4^+ concentration (Schjoerring et al., 1998a). The capacitance of the epicuticular water film is a function of the pH (see Sect. 3.1, Sutton et al., 1998), that is predominantly acidic (Flechard et al., 1999) and is taken as 4.5 (lower estimate) and as 4.0 (higher estimate) (cf. Sutton et al., 1998).

4.4.5. NH_3 flux from cattle excreta $F(NH_3)_{excreta}$:

In order to estimate the contribution of cattle excreta to the net NH_3 flux, we considered results of Boddey et al. (2004), who investigated the cycling of N in *Brachiaria* pastures in the south of the Brazilian province Bahia. According to their results, *Bos indicus* cattle excreted 37 kgN animal^{-1} yr^{-1} in manure and 49 kgN animal^{-1} yr^{-1} in urine when the pastures were stocked with two animals per hectare. The stocking rate at FNS was about one animal per hectare. About 8% of the excreted N may be released as NH_3 (L. Bouwman, personal communication, 2004). Hence, the average $F(NH_3)_{excreta}$ is estimated to be $\sim$10 ngN m^{-2} s^{-1}, which is applied for the entire measurement period (Eq. 5, 6).

4.5. Resistances, NH_3 canopy compensation point, transfer- and deposition velocities

4.5.1. The turbulent resistance R_a and the quasi-laminar boundary layer resistance R_b (Fig. 4a, b):

These resistances feature a typical diel variation with lowest values during daytime (R_a=20 s m^{-1}, R_b=30 s m^{-1}), because of strong turbulent mixing within the surface

EGU

layer, and higher values during nighttime (R_a=70 s m^{-1} and R_b=50 s m^{-1}).

4.5.2.   The bulk surface resistance R_c(NH$_3$) (Fig. 5):

The median diel cycle of the bulk surface resistance R_c(NH$_3$), that is the sum of the parallel resistances R_s(NH$_3$) and R_d(NH$_3$) (see Sect. 4.4) shows a pronounced diel fluctuation with higher values during sunlight hours and lower values at night. The upper estimate R_c(NH$_3$)_high (estimated from R_s(NH$_3$)_LE and R_d(NH$_3$)) varies between 20 and 60 s m^{-1} during daytime and is estimated to be <10 s m^{-1} during the night. The lower estimate R_c(NH$_3$)_low (estimated from R_c(O$_3$) and R_d(NH$_3$)) ranges from 100 to 200 s m^{-1} during the day and from 20 to 50 s m^{-1} during nighttime. Presumably, this diel pattern reflects the strong influence of nighttime epicuticular water layers on the surface uptake of NH$_3$.

4.5.3.   The NH$_3$ canopy compensation point concentration X$_c$(NH$_3$) (Fig. 6):

The X$_c$(NH$_3$) scenario for the dry season calculated according to Eq. (6) lies well within the range of values determined for grassland in other studies (Hesterberg et al., 1996; Meixner et al., 1996; Spindler et al., 2001; Sutton et al., 2001) and is a strong function of surface temperature (cf. Eqs. 6, 7). X$_c$(NH$_3$) is predicted to be particularly high at daytime, although low values of Γ were used to run the model. This is caused by prevailing high surface temperatures at the FNS pasture site (35–40°C at daytime and 20–25°C at night during the dry season). NH$_3$ deposits "and dissolves in" epicuticular water films at high *RHs* during nighttime. After sunrise when the surface temperature increases the NH$_3$ partial pressure above the epicuticular solution increases in accordance to Henry's law. This is visible in Fig. 6 as a distinctive peak of X$_c$(NH$_3$) after sunrise between 08:00 and 09:00 LT. Once most of the epicuticular NH$_4^+$ has evaporated, X$_c$(NH$_3$) subsequently decreases (after 09:00 LT). Lower surface temperatures during the transition period and the wet season have caused lower estimates of

N deposition in the tropics

I. Trebs et al.

EGU

$X_c(NH_3)$ (0.3–1 μg m^{-3} during nighttime and 1–4 μg m^{-3} during daytime).

4.5.4. Transfer- and deposition velocities $V_{tr.}(NH_3)$, $V_{tr.}(HONO)$, $V_d(HNO_3)$, $V_d(NO_2)$
(Fig. 7a–d) and V_p(aerosol) (Fig. 8):

For compounds featuring a bi-directional surface exchange the concept of a dry de-
position velocity V_d is no longer useful (e.g., Kramm and Dlugi, 1994). Thus, for bi-
directional NH$_3$ and HONO surface-atmosphere exchange the term transfer velocity
($V_{tr.}$) will be used henceforth.

The estimated upper median diel variation of $V_{tr.}(NH_3)$ (Fig. 7a) indicates net depo-
sition (= downward flux) at nighttime ($V_{tr.}(NH_3)$ >0) and net emission = upward flux
($V_{tr.}(NH_3)$ <0) during the day, whereas the lower estimate of $V_{tr.}(NH_3)$ shows only net
emission. Typically, $V_{tr.}(NH_3)$ is predicted to range between −1.5 cm s^{-1} during the
day and 1.0 cm s^{-1} at night for the upper estimate, and $V_{tr.}(NH_3)$ is estimated to vary
between −0.25 cm s^{-1} during the day and −1.0 cm s^{-1} at night for the lower estimate.
For cases of NH$_3$ net deposition, $V_{tr.}(NH_3)$ is in good agreement with values of 0.1–
2 cm s^{-1} observed by Erisman and Wyers (1993), Hesterberg et al. (1996), Nemitz et
al. (2004a), Phillips et al. (2004) and Rattray and Sievering (2001). For cases of NH$_3$
net emission, $V_{tr.}(NH_3)$ agrees well with values reported by e.g., Nemitz et al. (2004a).

The estimated median diel variation of $V_{tr.}(HONO)$ (Fig. 7b, dry season only) simi-
larly shows net deposition at night and net emission during the day, with $V_{tr.}(HONO)$
ranging from −1 cm s^{-1} to 1.3 cm s^{-1} (upper flux estimate) and between −0.5 cm s^{-1}
and 0.5 cm s^{-1} (lower flux estimate). For cases of HONO deposition, these values are
comparable to $V_{tr.}(HONO)$ of 0–1.7 cm s^{-1} reported by Harrison and Kitto (1994) and
Stutz et al. (2002).

The estimates of $V_d(HNO_3)$ shown in Fig. 7c, reveal maximal median values of 2.3 cm
s^{-1} at around 13:00 LT when $R_c(HNO_3)=1$ s m^{-1} is applied (see Table 3, upper flux es-
timate), coinciding with the period of highest turbulence. The lower estimate, when
$R_c(HNO_3)$ is taken as 50 s m^{-1} during daytime and as 15 s m^{-1} during nighttime

EGU

(see Table 3), results in median $V_d(HNO_3)$ values nearly equal during day and night ($\leq 1.1\,\text{cm s}^{-1}$), which is attributed to the compensating effect of lower surface uptake and low turbulent exchange during nighttime. Although $V_d(HNO_3)$ was found to be higher (3–4 cm s^{-1}) in other studies (e.g., Erisman et al., 1988), our values are still in reasonable agreement with deposition velocities determined by Dollard et al. (1987), Müller et al. (1993), Nemitz et al. (2004a) and Rattray and Sievering (2001) for vegetative canopies similar to that at FNS.

The median diel course of $V_d(NO_2)$ shown in Fig. 7d exhibits a less distinct pattern with maxima of ~0.4 cm s^{-1} during daytime. Values compare relatively well with $V_d(NO_2)$ reported by Kirkman et al. (2002); however, the dry deposition of NO_2 is thought to be mainly featured by uptake through plant stomata, which would imply that much higher dry deposition velocities (and hence much lower R_c) occur during daytime. As stated in Kirkman et al. (2002), measured day- and nighttime R_c values for NO_2 at FNS were similar, which was assumed to be mainly a result of stomatal closure due to high water vapor pressure deficit at lower *RH's* during daytime.

Deposition velocities V_p predicted for particles (Fig. 8) are estimated to be highest during daytime ($\leq 0.8\,\text{cm s}^{-1}$) in accordance with higher values of $u*$. During nighttime, V_p generally remains below 0.1 cm s^{-1}. As previously indicated, these values are much larger than V_p predicted by Slinn (1982) and are therefore considered as an upper estimate. It should be pointed out that aerosol water uptake at high *RHs* and the resulting particle growth during the deposition process may enhance deposition velocities (Khlystov, 1998; Gallagher et al., 1997). In our study, this would be particularly relevant for nighttime periods when *RH* usually exceeded 90%. However, a quantification of this effect would go beyond the scope of this work.

4.6. Surface-atmosphere exchange fluxes

In this section, the measured mixing ratios (Sect. 4.2), the input parameters for the inferential approach (discussed in Sect. 4.4) and the results presented in Sect. 4.5 will

EGU

be used to estimate and discuss surface-atmosphere exchange fluxes of N-containing trace gases and aerosol particles.

4.6.1. Bi-directional fluxes of gaseous NH_3 $F(NH_3)$ (Fig. 9a):

The application of the dynamic resistance model from (Sutton et al., 1998), which uses non-zero $X_c(NH_3)$ values and takes into account that deposited NH_3 may (re-)evaporate from surfaces, represents a rather conservative N deposition estimate (lower boundary). Since $X_c(NH_3)$ was assumed to be zero in several studies (Goulding et al., 1998; Russell et al., 2003; Singh et al., 2001; Tarnay et al., 2001), which implies that NH_3 is persistently net deposited to the surface (see Eq. 1), we have complemented the upper and lower bi-directional flux scenarios by additionally calculating a net deposition scenario for NH_3 (see Fig. 9a), assuming $X_c(NH_3)=0$ (Eq. 1) and using $R_c(NH_3)$_high (Fig. 5). Fluxes found at locations in temperate regions with vegetative surfaces similar to the grass surface at FNS are comparable to our upper bi-directional estimate of $F(NH_3)$ for the dry season (biomass burning) (Fig. 9a) (Erisman and Wyers, 1993; Flechard et al., 1999; Meixner et al., 1996; Spindler et al., 2001). The net emission peak between 08:00 and 09:30 LT in the upper estimate, corresponds to the peak of the predicted NH_3 canopy compensation point (cf. Fig. 6) and the highest observed NH_3 mixing ratios (see Fig. 2a). Relatively high median NH_3 net emission fluxes (5–70 ngN m^{-2} s^{-1}, upper estimate) during daytime (08:00–17:30 LT) are the result of (i.) relatively high NH_3 mixing ratios (Fig. 2a), (ii.) direct NH_3 emission from cattle excreta, (iii.) high surface temperatures and (iv.) corresponding high values of simulated $X_c(NH_3)$ (see Fig. 6). The simulated nighttime NH_3 net deposition (upper estimate) (19:00–06:30 LT) is on average -2–-13 ngN m^{-2} s^{-1}. The lower NH_3 flux estimate shown in Fig. 9a suggests that surface-atmosphere exchange of NH_3 may be significantly smaller when a higher epicuticular pH (4.5) (Sect. 4.4), a lower apoplastic $[NH_4^+]/[H^+]$ ratio Γ (Sect. 4.4) and lower $R_c(NH_3)$ (Fig. 5) are applied. The estimated NH_3 net deposition for this case during nighttime is negligible

N deposition in the tropics

I. Trebs et al.

Title Page

Abstract	Introduction
Conclusions	References
Tables	Figures

◄◄   ►►

◄   ►

| Back | Close |

Full Screen / Esc

Print Version

Interactive Discussion

EGU

and the predicted daytime NH_3 net emission varies between 1 and 20 ngN m^{-2} s^{-1}. During the transition period and the wet season, however, the lower NH_3 flux estimate (not shown) features emission during day and night. The NH_3 net deposition estimate (Fig. 9a) ($X_c(NH_3)=0$) exhibits highest fluxes during daytime (08:00–15:00 LT), with
5 values ranging between −20 and −40 ngN m^{-2} s^{-1}. At nighttime, net deposition fluxes between −5 and −20 ngN m^{-2} s^{-1} were estimated. Median $V_{tr}(NH_3)$ values for this case range from 0.5 to 1.5 cm s^{-1} (not shown).

The predicted bi-directional NH_3 flux scenarios are most sensitive to the pH of the epicuticular water film and the H^+ and NH_4^+ concentrations in the apoplastic fluid (Γ).
10 If the pH of the epicuticular water film would be >4.5 and Γ is constant (100–200), the upper NH_3 flux estimate would show net emission also during nighttime. On the other hand, increasing Γ beyond a value of 200 would result in daytime NH_3 net emissions significantly higher than observed in urban regions in Europe or North America.

4.6.2.   Bi-directional fluxes of gaseous HONO F(HONO) (Fig. 9b):

15 The estimated median diel HONO flux scenario during the dry season (12 to 23 September), shows a small net emission during the afternoon but net deposition of up to −1.3 ngN m^{-2} s^{-1} (upper estimate) from 17:00–08:40 LT. The net deposition for the lower flux estimate is smaller (≥−0.75 ngN m^{-2} s^{-1}) in accordance to higher values of $R_c(HONO)$ applied. We like to note, that the HONO flux scenario presented here
20 probably reflects the largest uncertainty of all flux estimates since presently neither $R_c(HONO)$ and $X_c(HONO)$, nor the exact HONO formation mechanism is well known.

4.6.3.   Fluxes of gaseous HNO$_3$ F(HNO$_3$) (Fig. 9c):

The estimated median diel HNO$_3$ flux scenario during the dry season is characterized by highest net deposition values from 09:00–16:30 LT (∼−0.5−−4 ngN m^{-2} s^{-1}, upper
25 estimate), coinciding with highest estimated deposition velocities (cf. Fig. 7c) and the maximal observed HNO$_3$ mixing ratios (cf. Fig. 2b). Predicted nighttime HNO$_3$ depo-

N deposition in the tropics

I. Trebs et al.

EGU

sition fluxes are lower in accordance with lower turbulence (lower V_d) and lower HNO_3 mixing ratios. The higher values of $R_c(HNO_3)$ applied for the lower flux estimate (Table 3) result in daytime net deposition fluxes that are a factor of two lower than for the upper flux estimate.

4.6.4. Fluxes of gaseous NO_2 $F(NO_2)$ (Fig. 9d):

The diel course of the estimated NO_2 flux (dry season) is always characterized by downward fluxes (net deposition). Median nighttime fluxes (18:00–08:00 LT) are at least two times higher than during the day (≥ -12 ngN m^{-2} s^{-1}). This is mainly due to generally higher NO_2 mixing ratios measured during nighttime (Fig. 2e) and a small diel variation of $V_d(NO_2)$ (see Fig. 7d), caused by similar day- and nighttime $R_c(NO_2)$ determined by (Kirkman et al., 2002).

4.6.5. Fluxes of aerosol NH_4^+ and NO_3 F(aerosol) (Fig. 10):

The estimated median diel flux of aerosol NH_4^+ for the dry season exhibits a net deposition pattern characterized by highest values just after 09:00 LT (~ -7 ngN m^{-2} s^{-1}), which is consistent with maximal aerosol NH_4^+ mixing ratios observed during this time (see Fig. 2g) and increased turbulent mixing (increasing u_*) after sunrise. Although aerosol NH_4^+ mixing ratios were generally lower during daytime, the dry deposition of aerosol NH_4^+ is estimated to be highest because of high V_p predicted during sunlight hours (see Fig. 8). The median diel course of the aerosol NO_3^- flux shown in Fig. 10 for the dry season resembles that estimated for aerosol NH_4^+, although the net deposition flux was at least three times lower than for aerosol NH_4^+, which is a consequence of lower aerosol NO_3^- mixing ratios (see Fig. 2g, h). The highest aerosol NO_3^- net deposition is predicted at around 09:00 LT (~ -2 ngN m^{-2} s^{-1}).

4.7. Seasonal cycles of dry and wet N deposition

Figure 11a, b illustrates the absolute amounts of the estimated monthly N deposition, whereby for dry N deposition (Fig. 11a) only cases of net deposition were considered. The dry deposition of NO_2 and total ammonium (NH_3 + aerosol NH_4^+) are estimated to be highest and decline by about 70% from September (late dry season, biomass burning) to November (onset of the wet season, clean conditions) (Fig. 11a). This indicates the influence of biomass burning during the dry season, which significantly enhances the dry deposition of NO_2 and NH_3. The dry deposition of total nitrate (HNO_3 + aerosol NO_3^-) also decreases by about 70% from September to November (Fig. 11a), but was on average 4 times lower than that of NO_2 and total ammonium. This is in accordance with lower mixing ratios observed for nitrate in gas and aerosol phase (Table 2) (cf. Trebs et al., 2004). The contribution of nitrite (HONO) to the dry deposition in September is smallest, and is negligible in October and November.

Obviously, wet N deposition (Fig. 11b) is substantially higher than dry N deposition at the FNS site. Wet N removal is dominated by ammonium and nitrate, and wet deposition of nitrite is at least 3 times smaller. Interestingly, the decrease of wet deposition of ammonium and nitrate from September to November is only ~20%, hence, much less pronounced than that for dry N deposition.

During the late dry season (biomass burning) in September, on average 44% of the total N deposition can be attributed to dry deposition and ~56% to wet deposition (Fig. 12a). With increasing rainfall amounts, the contribution of dry deposition drops to only 29% and 21% to the total N deposition during October (transition period) and November (onset of the wet season, clean conditions), respectively (Fig. 12b, c).

Dry N deposition at FNS was always dominated by NO_2 and NH_3. During September (dry season, Fig. 12a) the contribution of NO_2 and NH_3 to the total N deposition is estimated to be 18% and 16%, respectively. By contrast, the dry N deposition of HNO_3 and HONO is estimated to be small, contributing only 2.8% and 1.1% to the total N deposition during the dry season, respectively (Fig. 12a). Aerosol NH_4^+ and aerosol NO_3^-

show comparably small contributions to the total N deposition during the dry season (4.7% and 1.2%, respectively).

Through the transition period (October) until the wet season (November), the contribution of NO_2 dry deposition to the total deposition declines to about 10% (Fig. 12b, c).

5   The relative contribution of NH_3 to the total estimated N deposition decreases to 11% during the transition period and to 7.4% during the wet season. The dry N removal associated with HNO_3, HONO and aerosol NH_4^+ and NO_3^- is estimated to be negligibly small during the transition period and the wet season ($\leq$5% in total).

4.8.   Annual budget of surface-atmosphere exchange

10 The annual budget of surface-atmosphere exchange of inorganic N species at the FNS pasture site has been determined assuming that: (i.) September is representative for the entire dry season (May to September) (PM 10=100–200 μg m^{-3}), (ii.) October is representative for the two transition periods (April and October) (PM 10=50–100 μg m^{-3}), and (iii.) November is representative for the entire wet season (November to

15 March) (PM 10$\leq$25 μg m^{-3}) (Artaxo et al., 2002). The annual deposition of inorganic N species at the FNS pasture site is estimated to 7.3–9.8 kgN ha^{-1} yr^{-1}, whereof 2–4.5 kgN ha^{-1} yr^{-1} can be attributed to dry N deposition and ~5.3 kgN ha^{-1} yr^{-1} to wet N deposition. Thus, dry deposition may contribute on average 30% to the total annual N deposition. It is expected that 2.7–6.8 kgN ha^{-1} yr^{-1} are net (re-)emitted

20 in form of gaseous NH_3, HONO and NO from the pasture site (the annual estimate for net NO emission was taken from Kirkman et al., 2002), whereof at least 90% are expected to be in the form of NH_3. Regarding soil emission of nitrous oxide (N_2O), not included in this study, Garcia-Montiel et al. (2003) reported that the emission of N_2O from Amazonian pastures is even smaller than that of NO. Our study suggests that NH_3

25 is net emitted on an annual time scale, owing to high surface temperatures (efficient NH_3 emission through plant stomata) and direct NH_3 emission from cattle excreta. The total N budget at FNS is most sensitive to the modeled NH_3 flux. The FNS site may constitute an effective net sink of total inorganic N, if a zero-canopy compensation point

EGU

EGU

$X_c(NH_3)$ is assumed, or if $X_c(NH_3)$ is calculated using an epicuticular pH≤4.5 and a ratio of NH_4^+/H^+ in the apoplastic fluid Γ≤200.

Kirkman et al. (2002) reported that the FNS site constitutes a net NO_2 sink of 0.73 kgN ha^{-1} yr^{-1}. However, based on our measurements and considering $R_c(NO_2)$ determined by Kirkman et al. (2002), we calculated an annual NO_2 deposition of 1.24 kgN ha^{-1} yr^{-1}, which is nearly two times higher than the value derived by Kirkman et al. (2002). This discrepancy is most likely due to higher NO_2 mixing ratios observed during the dry (biomass burning) season in our study.

Moreover, it should be noted that water-soluble organic nitrogen (WSON) constitutes a significant part of the total N fraction of Amazonian aerosols. It was found by Mace et al. (2003), that organic N may represent 45% and 43% of the total N in wet and dry season aerosol samples, respectively. Obviously, the total deposition of atmospheric N would be significantly higher if these organic species were also taken into account.

Wet deposition of nitrate and ammonium in Central Amazonia was previously estimated to 1.7 kgN ha^{-1} yr^{-1}, 2.1 kgN ha^{-1} yr^{-1} and 2.8 kgN ha^{-1} yr^{-1} by Stallard and Edmond (1981), Andreae et al. (1990) and Williams et al. (1997), respectively. Since the measurement sites were situated in remote areas with less fire density, these estimates are about a factor of two lower than a value of 4.7 kgN ha^{-1} yr^{-1} (ammonium and nitrate only; nitrite excluded) obtained in this study.

Finally, Fig. 13 shows a comparison of our estimated N deposition with predictions by global chemistry and transport models (CTMs) (Bouwman et al., 2002; Dentener and Crutzen, 1994; Hauglustaine et al., 2004; Holland et al., 1997; Holland et al., 1999). The values from Dentener and Crutzen (1994) and Holland et al. (1997) are averages of N deposition predicted for the Amazon region (MOGUNTIA). The estimates from (Dentener and Crutzen, 1994) exclude dry deposition of NO_x and nitrate deposition. The value from Holland et al. (1999) (MOGUNTIA) represents predictions for tropical grasslands. Bouwman et al. (2002) (STOCHEM model) and Hauglustaine et al. (2004) (LMDz-INCA model) provide the total average N deposition for South America, which explains that their estimates are somewhat higher. Hauglustaine et al. (2004) do not

take into account surface (re-)emission of NH_3 ($X_c(NH_3)=0$). Not surprisingly, our N deposition estimate for the Amazonian pasture site is a factor of two to eight higher than model predictions for the Amazon region (Fig. 13).

5. Summary and conclusions

We have estimated dry and wet deposition of inorganic N at a tropical pasture site (Rondonia, Brazil) based on real-time measurements of inorganic N containing gases and aerosol species during the late dry (biomass burning) season, the transition period and the onset of the wet season (clean conditions) (LBA-SMOCC 2002). HNO_3, NO_2, aerosol NH_4^+ and NO_3^- were considered to be net deposited to the pasture site under all ambient conditions, while surface-atmosphere exchanges of HONO and NH_3 were considered to be of bi-directional nature. All fluxes have been determined by inferential techniques, making use of aerodynamic and surface related resistances that have been deduced from measurements or were taken from recent literature. For the least-well defined quantities, lower and upper cases have been considered. Bi-directional NH_3 fluxes were predicted using a dynamic resistance model from Sutton et al. (1998). NO_2 and NH_3 are the most important contributors to dry N deposition and their fluxes largely control the total dry N deposition pattern at the pasture site. Mixing ratios of NO_2 and water-soluble N species in gas and aerosol phase are significantly enhanced when widespread biomass burning takes place during the dry season, resulting in high N deposition rates. The contribution of the dry N deposition to the total N deposition decreased substantially from the dry (biomass burning) season to the wet season. The estimated total (dry + wet) N deposition to this tropical pasture site is 7.3–9.8 kgN ha^{-1} yr^{-1}, whereof 2–4.5 kgN ha^{-1} yr^{-1} are attributed to dry N deposition and $\sim$5.3 kgN ha^{-1} yr^{-1} to wet N deposition. Thus, dry deposition may contribute on average 30% to the total N deposition. It is expected that 2.7–6.8 kgN ha^{-1} yr^{-1} are net (re-)emitted from the pasture site, mainly in the form of NH_3. The largest uncertainties in our estimates are (i.) the epicuticular pH and (ii.) the ratio of NH_4^+ and H^+ concentration in the apoplastic

[ACPD](#)

5, 3131–3189, 2005

N deposition in the tropics

I. Trebs et al.

Title Page

Abstract	Introduction
Conclusions	References
Tables	Figures

Back | Close

Full Screen / Esc

Print Version

Interactive Discussion

EGU

fluid (Γ). These quantities strongly control the NH_3 canopy compensation point concentration and, hence, the estimated bi-directional NH_3 flux. In this study, low values of (i.) the epicuticular pH (4–4.5) and (ii.) the ratio of NH_4^+ and H^+ concentration in the apoplastic fluid (Γ=100–200) were assumed. The latter can be justified by the low soil N status of the pasture, and, in combination with a low epicuticular pH, the daytime net emission and nighttime net deposition pattern of the NH_3 flux found in temperate latitudes could be reproduced. Our results suggest that – regardless of considering net deposition of NH_3 or bi-directional NH_3 exchange – the contemporary net N deposition to tropical ecosystems predicted by global CTMs may be underestimated at least by a factor of two. Up to now, approximately 15% of the original Amazonian rainforest has been deforested and was mostly converted to cattle pastures. Our N deposition estimate is suggested to be representative for these areas, featuring comparable land use patterns and microclimates. N deposition in these regions may therefore be comparable to moderately polluted urban regions in e.g., North America (Munger et al., 1998; Tarnay et al., 2001).

EGU

References

Alicke, B., Geyer, A., Hofzumahaus, A., Holland, F., Konrad, S., Patz, H. W., Schafer, J., Stutz, J., Volz-Thomas, A., and Platt, U.: OH formation by HONO photolysis during the BERLIOZ experiment, J. Geophys. Res.-A, 108, 8247, doi:8210.1029/2001JD000579, 2003.

Ammann, C.: On the applicability of relaxed eddy accumulation and common methods for measuring trace gas fluxes. Zürcher Geopgraphische Schriften, ETH, Zürich, 1–50, 1999.

Andreae, M. O., Artaxo, P., Brandao, C., Carswell, F. E., Ciccioli, P., da Costa, A. L., Culf, A. D., Esteves, J. L., Gash, J. H. C., Grace, J., Kabat, P., Lelieveld, J., Malhi, Y., Manzi, A. O., Meixner, F. X., Nobre, A. D., Nobre, C., Ruivo, M., Silva-Dias, M. A., Stefani, P., Valentini, R., von Jouanne, J., and Waterloo, M. J.: Biogeochemical cycling of carbon, water, energy, trace gases, and aerosols in Amazonia: The LBA-EUSTACH experiments, J. Geophys. Res.-A, 107, 8066, doi:8010.1029/2001JD000524, 2002.

Andreae, M. O., Talbot, R. W., Berresheim, H., and Beecher, K. M.: Precipitation Chemistry in Central Amazonia, J. Geophys. Res.-A, 95, 16 987–16 999, 1990.

Araujo, A. C., Nobre, A. D., Kruijt, B., Elbers, J. A., Dallarosa, R., Stefani, P., von Randow, C., Manzi, A. O., Culf, A. D., Gash, J. H. C., Valentini, R., and Kabat, P.: Comparative measurements of carbon dioxide fluxes from two nearby towers in a central Amazonian rainforest: The Manaus LBA site, J. Geophys. Res.-A, 107(D20), 8090, doi:10.1029/2001JD000676, 2002.

Artaxo, P., Martins, J. V., Yamasoe, M. A., Procopio, A. S., Pauliquevis, T. M., Andreae, M. O., Guyon, P., Gatti, L. V., and Leal, A. M. C.: Physical and chemical properties of aerosols in the wet and dry seasons in Rondonia, Amazonia, J. Geophys. Res.-A, 107(D20), 8081, doi:10.1029/2001JD000666, 2002.

Asner, G. P., Townsend, A. R., Riley, W. J., Matson, P. A., Neff, J. C., and Cleveland, C. C.: Physical and biogeochemical controls over terrestrial ecosystem responses to nitrogen deposition, Biogeochemistry, 54, 1–39, 2001.

Boddey, R. M., Macedo, R., Tarre, R. M., Ferreira, E., de Oliveira, O. C., Rezende, C. D., Cantarutti, R. B., Pereira, J. M., Alves, B. J. R., and Urquiaga, S.: Nitrogen cycling in Brachiaria pastures: the key to understanding the process of pasture decline, Agriculture Ecosystems & Environment, 103, 389–403, 2004.

Bouwman, A. F., Van Vuuren, D. P., Derwent, R. G., and Posch, M.: A global analysis of acidification and eutrophication of terrestrial ecosystems, Water, Air, Soil, Pollut., 141, 349–

EGU

382, 2002.

Brunnemann, G., Kins, L., and Dlugi, R.: Physical and chemical characterisation of the atmospheric aerosol: An overview of the measurements during the SANA 2 campaign at Melpitz, Meteorologische Zeitschrift, N.F., 5, 245–256, 1996.

5 Clark, K. L., Nadkarni, N. M., Schaefer, D., and Gholz, H. L.: Atmospheric deposition and net retention of ions by the canopy in a tropical montane forest, Monteverde, Costa Rica, J. Trop. Ecol., 14, 27–45, 1998.

Culf, A. D., Esteves, J. L., de O. Marques Filho, A., and Da Rocha, H. R.: Radiation, temperature and humidity over forest and pasture in Amazonia, Amazonian Deforestation and Climate,
10 edited by: Gash, J. H. C., Nobre, C. A., Roberts, J. M., and Victoria, R. L., New York, John Wiley, 413–424, 1996.

Davidson, E. A., Carvalho, C. J. R., Vieira, I. C. G., Figueiredo, R. O., Moutinho, P., Ishida, F. Y., dos Santos, M. T. P., Guerrero, J. B., Kalif, K., and Sabá, R. T.: Nutrient limitation of biomass growth in a tropical secondary forest: Early results of a nitrogen and phosphorus
15 amendment experiment, Ecological Applications, in press, 2005.

De Arellano, J. V.-G. and Duynkerke, P. G.: Influence of Chemistry on the Flux-Gradient Relationships for the NO-O3-NO2 System, Boundary-Layer Meteorology, 61, 375–387, 1992.

Dentener, F. J. and Crutzen, P. J.: A 3-Dimensional Model of the Global Ammonia Cycle, J. Atmos. Chem., 19, 331–369, 1994.

20 Dlugi, R.: Interaction of NOx and VOCs within vegetation, Photo-oxidants: Precursors and Products, Proceedings of EUROTRAC Symposium '92, edited by: Borrell, P. B. P. M., Cvitas, T., and Seiler, W., The Hague, Academic Publishing, 682–688, 1993.

Dollard, G. J., Atkins, D. H. F., Davies, T. J., and Healy, C.: Concentrations and Dry Deposition Velocities of Nitric-Acid, Nature, 326, 481–483, 1987.

25 Erisman, J. W., Vanpul, A., and Wyers, P.: Parametrization of Surface-Resistance for the Quantification of Atmospheric Deposition of Acidifying Pollutants and Ozone, Atmos. Environ., 28, 2595–2607, 1994.

Erisman, J. W., Vermetten, A. W. M., Asman, W. A. H., Waijers-Ijpelaan, A., and Slanina, J.: Vertical-Distribution of Gases and Aerosols – the Behavior of Ammonia and Related
30 Components in the Lower Atmosphere, Atmos. Environ., 22, 1153–1160, 1988.

Erisman, J. W. and Wyers, G. P.: Continuous Measurements of Surface Exchange of SO_2 and NH_3 – Implications for Their Possible Interaction in the Deposition Process, Atmos. Environ. Part a-General Topics, 27, 1937–1949, 1993.

N deposition in the tropics

I. Trebs et al.

EGU

Falkovich, A. H., Graber, E. R., Schkolnik, G., Rudich, Y., Maenhaut, W., and Artaxo, P.: Low molecular weight organic acids in aerosol particles from Rondônia, Brazil, during the biomass-burning, transition and wet periods, Atmos. Chem. Phys., 5, 781–797, 2005, SRef-ID: 1680-7324/acp/2005-5-781.

5   Farquhar, G. D., Firth, P. M., Wetselaar, R., and Weir, B.: On the Gaseous Exchange of Ammonia between Leaves and the Environment – Determination of the Ammonia Compensation Point, Plant Physiology, 66, 710–714, 1980.

Fehsenfeld, F. C., Drummond, J. W., Roychowdhury, U. K., Galvin, P. J., Williams, E. J., Buhr, M. P., Parrish, D. D., Hubler, G., Langford, A. O., Calvert, J. G., Ridley, B. A., Grahek, F., Heikes,

10   B. G., Kok, G. L., Shetter, J. D., Walega, J. G., Elsworth, C. M., Norton, R. B., Fahey, D. W., Murphy, P. C., Hovermale, C., Mohnen, V. A., Demerjian, K. L., Mackay, G. I., and Schiff, H. I.: Intercomparison of No2 Measurement Techniques, J. Geophys. Res.-A, 95, 3579–3597, 1990.

Fisch, G., Tota, J., Machado, L. A. T., Dias, M., Lyra, R. F. D., Nobre, C. A., Dolman, A. J., and

15   Gash, J. H. C.: The convective boundary layer over pasture and forest in Amazonia, Theor. Appl. Climatol., 78, 47–59, 2004.

Flechard, C. R., Fowler, D., Sutton, M. A., and Cape, J. N.: A dynamic chemical model of bi-directional ammonia exchange between semi-natural vegetation and the atmosphere, Q. J. Roy. Meteor. Soc., 125, 2611–2641, 1999.

20   Gallagher, M. W., Fontan, J., Wyers, G. P., Ruijgrok, W., Duyzer, J., Hummelshoj, P., Pile-gaard, K., and Fowler, D.: Atmospheric particles and their interactions with natural surfaces, Biosphere-Atmosphere Exchange of Pollutants and Trace substances EUROTRAC-BIATEX, J. Slanina, Springer, 4, 45–92, 1997.

Galloway, J. N.: The global nitrogen cycle: changes and consequences, Environ. Pollut., 102,

25   15–24, 1998.

Galloway, J. N., Likens, G. E., Keene, W. C., and Miller, J. M.: The Composition of Precipitation in Remote Areas of the World, J. Geophys. Res., 87, 8771–8786, 1982.

Garcia-Montiel, D. C., Steudler, P. A., Piccolo, M., Neill, C., Melillo, J., and Cerri, C. C.: Nitrogen oxide emissions following wetting of dry soils in forest and pastures in Rondonia, Brazil,

30   Biogeochemistry, 64, 319–336, 2003.

Garland, J. A.: On the size dependence of particle deposition, Water, Air and Soil Pollution: Focus, 1 (5-6), 323–332, 2001.

Garratt, J. R.: The atmospheric boundary layer, Cambridge, 315, Cambridge University Press,

EGU

1992.

Goulding, K. W. T., Bailey, N. J., Bradbury, N. J., Hargreaves, P., Howe, M., Murphy, D. V., Poulton, P. R., and Willison, T. W.: Nitrogen deposition and its contribution to nitrogen cycling and associated soil processes, New Phytologist, 139, 49–58, 1998.

Hall, S. J. and Matson, P. A.: Nitrogen oxide emissions after nitrogen additions in tropical forests, Nature, 400, 152–155, 1999.

Hanson, P. J. and Lindberg, S. E.: Dry Deposition of Reactive Nitrogen-Compounds – a Review of Leaf, Canopy and Non-Foliar Measurements, Atmos. Environ. Part a-General Topics, 25, 1615–1634, 1991.

Harrison, R. M. and Kitto, A. M. N.: Evidence for a Surface Source of Atmospheric Nitrous-Acid, Atmos. Environ., 28, 1089–1094, 1994.

Harrison, R. M., Peak, J. D., and Collins, G. M.: Tropospheric cycle of nitrous acid, J. Geophys. Res.-A, 101, 14 429–14 439, 1996.

Harrison, R. M., Sturges, W. T., Kitto, A. M. N., and Li, Y. Q.: Kinetics of Evaporation of Ammonium-Chloride and Ammonium-Nitrate Aerosols, Atmos. Environ. Part a-General Topics, 24, 1883–1888, 1990.

Hauglustaine, D. A., Hourdin, F., Jourdain, L., Filiberti, M. A., Walters, S., Lamarque, J. F., and Holland, E. A.: Interactive chemistry in the Laboratoire de Meteorologie Dynamique general circulation model: Description and background tropospheric chemistry evaluation, J. Geophys. Res.-A, 109, D04314, doi:10.1029/2003JD003957, 2004.

Hesterberg, R., Blatter, A., Fahrni, M., Rosset, M., Neftel, A., Eugster, W., and Wanner, H.: Deposition of nitrogen-containing compounds to an extensively managed grassland in central Switzerland, Environ. Pollut., 91, 21–34, 1996.

Hicks, B. B., Baldocchi, D. D., Meyers, T. P., Hosker, R. P., and Matt, D. R.: A Preliminary Multiple Resistance Routine for Deriving Dry Deposition Velocities from Measured Quantities, Water, Air, Soil Poll., 36, 311–330, 1987.

Holland, E. A., Braswell, B. H., Lamarque, J. F., Townsend, A., Sulzman, J., Muller, J. F., Dentener, F., Brasseur, G., Levy, H., Penner, J. E., and Roelofs, G. J.: Variations in the predicted spatial distribution of atmospheric nitrogen deposition and their impact on carbon uptake by terrestrial ecosystems, J. Geophys. Res.-A, 102, 15 849–15 866, 1997.

Holland, E. A., Dentener, F. J., Braswell, B. H., and Sulzman, J. M.: Contemporary and pre-industrial global reactive nitrogen budgets, Biogeochemistry, 46, 7–43, 1999.

Howarth, R. W., Billen, G., Swaney, D., Townsend, A., Jaworski, N., Lajtha, K., Downing, J. A.,

Title Page

Abstract | Introduction

Conclusions | References

Tables | Figures

◄ | ►

◄ | ►

Back | Close

Full Screen / Esc

Print Version

Interactive Discussion

EGU

Elmgren, R., Caraco, N., Jordan, T., Berendse, F., Freney, J., Kudeyarov, V., Murdoch, P., and Zhu, Z. L.: Regional nitrogen budgets and riverine N&P fluxes for the drainages to the North Atlantic Ocean: Natural and human influences, Biogeochemistry, 35, 75–139, 1996.

Huebert, B. J. and Robert, C. H.: The Dry Deposition of Nitric-Acid to Grass, J. Geophys. Res.-A, 90, 2085–2090, 1985.

Kauffman, J. B., Cummings, D. L., and Ward, D. E.: Fire in the Brazilian Amazon 2. Biomass, nutrient pools and losses in cattle pastures, Oecologia, 113, 415–427, 1998.

Kauffman, J. B., Cummings, D. L., Ward, D. E., and Babbitt, R.: Fire in the Brazilian Amazon 1. Biomass, Nutrient Pools, and Losses in Slashed Primary Forests, Oecologia, 104, 397–408, 1995.

Khlystov, A.: Cloud forming properties of ambient aerosol in the Netherlands and resultant shortwave radiative forcing of climate, Dept. of acgricultural sciences, Wageningen, University of Wageningen, 1998.

Khlystov, A., Wyers, G. P., and Slanina, J.: The Steam-Jet Aerosol Collector, Atmos. Environ., 29, 2229–2234, 1995.

Kirkman, G. A., Gut, A., Ammann, C., Gatti, L. V., Cordova, A. M., Moura, M. A. L., Andreae, M. O., and Meixner, F. X.: Surface exchange of nitric oxide, nitrogen dioxide, and ozone at a cattle pasture in Rondonia, Brazil, J. Geophys. Res.-A, 107, 8083, doi:8010.1029/2001JD000523, 2002.

Kramm, G. and Dlugi, R.: Modeling of the Vertical Fluxes of Nitric-Acid, Ammonia, and Ammonium-Nitrate, J. Atmos. Chem., 18, 319–357, 1994.

Kraus, A. and Hofzumahaus, A.: Field measurements of atmospheric photolysis frequencies for O-3, NO2, HCHO, CH3CHO, H2O2, and HONO by UV spectroradiometry, J. Atmos. Chem., 31, 161–180, 1998.

Lammel, G. and Cape, J. N.: Nitrous acid and nitrite in the atmosphere, Chemical Society Reviews, 25, 361–369, 1996.

Lara, L., Artaxo, P., Martinelli, L. A., Victoria, R. L., Camargo, P. B., Krusche, A., Ayers, G. P., Ferraz, E. S. B., and Ballester, M. V.: Chemical composition of rainwater and anthropogenic influences in the Piracicaba River Basin, Southeast Brazil, Atmos. Environ., 35, 4937–4945, 2001.

Lenschow, D. H.: Reactive trace species in the boundary layer from a micrometeorological perspective, J. Meteorol. Soc. Jpn., 60, 161–172, 1982.

Lesack, L. F. W. and Melack, J. M.: The Deposition, Composition, and Potential Sources of

N deposition in the tropics

I. Trebs et al.

Title Page

Abstract	Introduction
Conclusions	References
Tables	Figures

◀ ▶

◀ ▶

| Back | Close |

Full Screen / Esc

Print Version

Interactive Discussion

EGU

Major Ionic Solutes in Rain of the Central Amazon Basin, Water Resour. Res., 27, 2953–2977, 1991.

Likens, G. E., Keene, W. C., Miller, J. M., and Galloway, J. N.: Chemistry of Precipitation from a Remote, Terrestrial Site in Australia, J. Geophys. Res.-A, 92, 13 299–13 314, 1987.

Loubet, B., Milford, C., Hill, P. W., Tang, Y. S., Cellier, P., and Sutton, M. A.: Seasonal variability of apoplastic NH4+ and pH in an intensively managed grassland, Plant and Soil, 238, 97–110, 2002.

Mace, K. A., Artaxo, P., and Duce, R. A.: Water-soluble organic nitrogen in Amazon Basin aerosols during the dry (biomass burning) and wet seasons, J. Geophys. Res.-A, 108, 4512, doi:4510.1029/2003JD003557, 2003.

Matson, P. A., McDowell, W. H., Townsend, A. R., and Vitousek, P. M.: The globalization of N deposition: ecosystem consequences in tropical environments, Biogeochemistry, 46, 67–83, 1999.

Meixner, F. X.: Surface exchange of odd nitrogen oxides, Nova Acta Leopoldina, 70, 299–348, 1994.

Meixner, F. X., Wyers, G. P., and Neftel, A.: Bi-directional exchange of ammonia over cereals, Proceedings of EUROTRAC Symposium '96, edited by: Borrell, P. B. P. M., Cvitas, T., Kelly, K., and Seiler, W., Southhampton, Computational Mechanics Publications, 1996.

Meng, Z. Y. and Seinfeld, J. H.: Time scales to achieve atmospheric gas-aerosol equilibrium for volatile species, Atmos. Environ., 30, 2889–2900, 1996.

Müller, H., Kramm, G., Meixner, F., Dollard, G. J., Fowler, D., and Possanzini, M.: Determination of HNO3 Dry Deposition by Modified Bowen-Ratio and Aerodynamic Profile Techniques, Tellus Series B-Chemical and Physical Meteorology, 45, 346–367, 1993.

Munger, J. W., Fan, S. M., Bakwin, P. S., Goulden, M. L., Goldstein, A. H., Colman, A. S., and Wofsy, S. C.: Regional budgets for nitrogen oxides from continental sources: Variations of rates for oxidation and deposition with season and distance from source regions, J. Geophys. Res.-A, 103, 8355–8368, 1998.

Nemitz, E., Sutton, M. A., Wyers, G. P., and Jongejan, P. A. C.: Gas-particle interactions above a Dutch heathland: I. Surface exchange fluxes of NH3, SO2, HNO3 and HCl, Atmos. Chem. Phys., 4, 989–1005, 2004a,
SRef-ID: 1680-7324/acp/2004-4-989.

Nemitz, E., Sutton, M. A., Wyers, G. P., Otjes, R. P., Mennen, M. G., van Putten, E. M., and Gallagher, M. W.: Gas-particle interactions above a Dutch heathland: II. Concentrations

EGU

and surface exchange fluxes of atmospheric particles, Atmos. Chem. Phys., 4, 1007–1024, 2004b,
SRef-ID: 1680-7324/acp/2004-4-1007.

Nicholson, K. W.: The Dry Deposition of Small Particles – a Review of Experimental Measurements, Atmos. Environ., 22, 2653–2666, 1988.

Nobre, C. A., Fisch, G., da Rocha, H. R., Lyra, R. F. D., da Rocha, E. P., da Costa, A. C. L., and Ubarana, V. N.: Observations of the atmospheric boundary layer in Rondônia, Amazonian Deforestation and Climate, edited by: Gash, J. H. C., Nobre, C. A., Roberts, J. M., and Victoria, R. L., New York, John Wiley, 413–424, 1996.

Oliveira, O. C., Oliveira, I. P. d., Ferreira, E., Alves, B. J. R., Miranda, C. H. B., Vilela, L., Urquiaga, S., and Boddey, R. M.: Response of degraded pastures in the Brazilian Cerrado to chemical fertilisation, Pasturas Tropicales, 23, 14–18, 2001.

Pandis, S. N., Wexler, A. S., and Seinfeld, J. H.: Dynamics of Tropospheric Aerosols, J. Phys. Chem., 99, 9646–9659, 1995.

Phillips, S. B., Arya, S. P., and Aneja, V. P.: Ammonia Flux and dry deposition velocity from near-surface concentration gradient measurements over a grass surface in North Carolina, Atmos. Environ., 38, 3469–3480, 2004.

Rattray, G. and Sievering, H.: Dry deposition of ammonia, nitric acid, ammonium, and nitrate to alpine tundra at Niwot Ridge, Colorado, Atmos. Environ., 35, 1105–1109, 2001.

Reid, J. S. and Hobbs, P. V.: Physical and optical properties of young smoke from individual biomass fires in Brazil, J. Geophys. Res.-A, 103, 32 013–32 030, 1998.

Reiners, W. A., Liu, S., Gerow, K. G., Keller, M., and Schimel, D. S.: Historical and future land use effects on N2O and NO emissions using an ensemble modeling approach: Costa Rica's Caribbean lowlands as an example, Global Biogeochem. Cycles, 16 (4), 1068, doi:10.1029/2001GB001437, 2002.

Rissler, J., Swietlicki, E., Zhou, J., Roberts, G., Andreae, M. O., Gatti, L. V., and Artaxo, P.: Physical properties of the sub-micrometer aerosol over the Amazon rain forest during the wet-to-dry season transition – comparison of modeled and measured CCN concentrations, Atmos. Chem. Phys., 4, 2119–2143, 2004,
SRef-ID: 1680-7324/acp/2004-4-2119.

Ruijgrok, W., Davidson, C. I., and Nicholson, K. W.: Dry Deposition of Particles – Implications and Recommendations for Mapping of Deposition over Europe, Tellus Series B-Chemical and Physical Meteorology, 47, 587–601, 1995.

N deposition in the tropics

I. Trebs et al.

Title Page

Abstract	Introduction
Conclusions	References
Tables	Figures

◄ | ►

◄ | ►

Back | Close

Full Screen / Esc

Print Version

Interactive Discussion

EGU

Russell, K. M., Keene, W. C., Maben, J. R., Galloway, J. N., and Moody, J. L.: Phase partitioning and dry deposition of atmospheric nitrogen at the mid-Atlantic US coast, J. Geophys. Res.-A, 108(D21), 4656, doi:10.1029/2003JD003736, 2003.

Schiemang, R., Kleist, E., Kleffman, J., and Wildt, J.: Uptake of nitrous acid (HONO) by plants, Geophys. Res. Abstr., 6, SRef-ID: 1607-7962/gra/EGU1604-A-02812, 2004.

Schjoerring, J. K., Husted, S., and Mattsson, M.: Physiological parameters controlling plant-atmosphere ammonia exchange, Atmos. Environ., 32, 491–498, 1998a.

Seidl, W., Brunnemann, G., Kins, L., Köhler, E., Reuswig, K., and Dlugi, R.: On the ionic composition of aerosol particles and related gas phase species at two sites during the SANA 2 campaign, Meteorologische Zeitschrift, N.F., 5, 257–268, 1996.

Seinfeld, J. H. and Pandis, S. N.: Atmospheric Chemistry and Physics, New York, John Wiley & Sons, Inc., 1998.

Singh, S. P., Satsangi, G. S., Khare, P., Lakhani, A., Maharaj Kumari, K., and Srivastava, S. S.: Multiphase measurement of atmospheric ammonia, Atmos. Environ., 3, 107–116, 2001.

Slanina, J., ten Brink, H. M., Otjes, R. P., Even, A., Jongejan, P., Khlystov, A., Waijers-Ijpelaan, A., and Hu, M.: The continuous analysis of nitrate and ammonium in aerosols by the steam jet aerosol collector (SJAC): extension and validation of the methodology, Atmos. Environ., 35, 2319–2330, 2001.

Slinn, W. G. N.: Predictions for Particle Deposition to Vegetative Canopies, Atmos. Environ., 16, 1785–1794, 1982.

Spindler, G., Teichmann, U., and Sutton, M. A.: Ammonia dry deposition over grassland – micrometeorological flux-gradient measurements and bidirectional flux calculations using an inferential model, Q. J. Roy. Meteor. Soc., 127, 795–814, 2001.

Srivastava, A. K. and Ambasht, R. S.: Nitrogen Deposition in Casuarina-Equisetifolia (Forst) Plantation Stands in the Dry Tropics of Sonbhadra, India, Forest Ecology and Management, 70, 341–348, 1994.

Stallard, R. F. and Edmond, J. M.: Geochemistry of the Amazon 1. Precipitation Chemistry and the Marine Contribution to the Dissolved-Load at the Time of Peak Discharge, J. Geophys. Res., 86, 9844–9858, 1981.

Stutz, J., Alicke, B., and Neftel, A.: Nitrous acid formation in the urban atmosphere: Gradient measurements of NO2 and HONO over grass in Milan, Italy, J. Geophys. Res.-A, 107, 8192, doi:8110.1029/2001JD000390, 2002.

Sutton, M. A., Asman, W. A. H., and Schjorring, J. K.: Dry Deposition of Reduced Nitrogen,

N deposition in the tropics

I. Trebs et al.

Title Page

Abstract	Introduction
Conclusions	References
Tables	Figures

◄ | ►|

◄ | ►

Back | Close

Full Screen / Esc

Print Version

Interactive Discussion

EGU

Tellus Series B-Chemical and Physical Meteorology, 46, 255–273, 1994.

Sutton, M. A., Burkhardt, J. K., Guerin, D., Nemitz, E., and Fowler, D.: Development of resistance models to describe measurements of bi-directional ammonia surface-atmosphere exchange, Atmos. Environ., 32, 473–480, 1998.

Sutton, M. A., Milford, C., Nemitz, E., Theobald, M. R., Hill, P. W., Fowler, D., Schjoerring, J. K., Mattsson, M. E., Nielsen, K. H., Husted, S., Erisman, J. W., Otjes, R., Hensen, A., Mosquera, J., Cellier, P., Loubet, B., David, M., Genermont, S., Neftel, A., Blatter, A., Herrmann, B., Jones, S. K., Horvath, L., Fuhrer, E. C., Mantzanas, K., Koukoura, Z., Gallagher, M., Williams, P., Flynn, M., and Riedo, M.: Biosphere-atmosphere interactions of ammonia with grasslands: Experimental strategy and results from a new European initiative, Plant and Soil, 228, 131–145, 2001.

Tarnay, L., Gertler, A. W., Blank, R. R., and Taylor, G. E.: Preliminary measurements of summer nitric acid and ammonia concentrations in the Lake Tahoe Basin air-shed: implications for dry deposition of atmospheric nitrogen, Environ. Pollut., 113, 145–153, 2001.

Thom, A. S.: Vegetation and the atmosphere, Momentum, mass and heat exchange, edited by: Moneith, J. L., Chichester, UK, Academic Press, 57–109, 1975.

Townsend, A. R., Braswell, B. H., Holland, E. A., and Penner, J. E.: Spatial and temporal patterns in terrestrial carbon storage due to deposition of fossil fuel nitrogen, Ecological Applications, 6, 806–814, 1996.

Trebs, I., Meixner, F. X., Slanina, J., Oties, R. P., Jongejan, P., and Andreae, M. O.: Real-time measurements of ammonia, acidic trace gases and water-soluble inorganic aerosol species at a rural site in the Amazon Basin, Atmos. Chem. Phys., 4, 967–987, 2004, SRef-ID: 1680-7324/acp/2004-4-967.

Trebs, I., Metzger, S., Meixner, F. X., Helas, G., Andreae, M. O., Moura, M. A. L., Da Silva, R. J., Slanina, J., Rudich, Y., Falkovich, A., and Artaxo, P.: The $NH_4^+ - NO_3^- - Cl^- - SO_4^{2-} - H_2O$ system and its gas phase precursors at a pature site in the Amazon Basin: How relevant are mineral cations and soluble organic acids?, J. Geophys. Res.-A, 110(D07303), doi:10.1029/2004JD005478, 2005.

van Hove, L. W. A., Heeres, P., and Bossen, M. E.: The annual variation in stomatal ammonia compensation point of rye grass (Lolium perenne L.) leaves in an intensively managed grassland, Atmos. Environ., 36, 2965–2977, 2002.

Vitousek, P. M., Aber, J. D., Howarth, R. W., Likens, G. E., Matson, P. A., Schindler, D. W., Schlesinger, W. H., and Tilman, D. G.: Human alteration of the global nitrogen cycle: Sources

and consequences, Ecological Applications, 7, 737–750, 1997.

Vong, R. J., Vickers, D., and Covert, D. S.: Eddy correlation measurements of aerosol deposition to grass, Tellus Series B-Chemical and Physical Meteorology, 56, 105–117, 2004.

Wesely, M. L.: Parameterization of Surface Resistances to Gaseous Dry Deposition in Regional-Scale Numerical-Models, Atmos. Environ., 23, 1293–1304, 1989.

Wesely, M. L., Cook, D. R., Hart, R. L., and Speer, R. E.: Measurements and Parameterization of Particulate Sulfur Dry Deposition over Grass, J. Geophys. Res.-A, 90, 2131–2143, 1985.

Wesely, M. L. and Hicks, B. B.: Some Factors That Affect Deposition Rates of Sulfur-Dioxide and Similar Gases on Vegetation, JAPCA J. Air Waste Ma., 27, 1110–1116, 1977.

Wesely, M. L. and Hicks, B. B.: A review of the current status of knowledge on dry deposition, Atmos. Environ., 34, 2261–2282, 2000.

Wexler, A. S. and Seinfeld, J. H.: The Distribution of Ammonium-Salts among a Size and Composition Dispersed Aerosol, Atmos. Environ. Part A-General Topics, 24, 1231–1246, 1990.

Wexler, A. S. and Seinfeld, J. H.: Analysis of Aerosol Ammonium-Nitrate – Departures from Equilibrium During SCAQS, Atmos. Environ. Part a-General Topics, 26, 579–591, 1992.

Williams, M. R., Fisher, T. R., and Melack, J. M.: Chemical composition and deposition of rain in the central Amazon, Brazil, Atmos. Environ., 31, 207–217, 1997.

Wyers, G. P., Otjes, R. P., and Slanina, J.: A Continuous-Flow Denuder for the Measurement of Ambient Concentrations and Surface-Exchange Fluxes of Ammonia, Atmos. Environ. Part a-General Topics, 27, 2085–2090, 1993.

EGU

N deposition in the tropics

I. Trebs et al.

EGU

Table 1. Specifications of the instrumentation for the measurement of trace gases, aerosol species and (micro)-meteorological quantities at FNS during LBA-SMOCC 2002 (all heights are above ground).

Parameter/position/ height	Time resolution	Technique or sensor	Model, manufacturer	Detection limit/ precision
NH_3, HNO_3, HONO *(5.3 m)*	20–60 min [1]	Wet-annular denuder (WAD), IC, FIA[2]	ECN, Petten, Netherlands	≤0.015 ppb (3σ) for acids, ≤0.118 ppb (3σ) for NH_3
Aerosol NH_4^+, NO_3^- *(5.3 m)*	20–60 min	Steam-Jet Aerosol Collector (SJAC), IC, FIA	ECN, Petten, Netherlands	≤0.015 ppb (3σ) for anions, ≤0.118 ppb (3σ) for aerosol NH_4^+
NO concentration *(10 m)*	5 min	Gas-phase chemiluminescense	Model 42C TL (trace level),Thermo Environment Instruments Inc., USA	0.05±0.025 ppb
NO_2 concentration *(10 m)*	5 min	Catalytic conversion of NO_2 to NO by molybdenum converter (at 325°C), gas phase chemiluminescence	Model 42C TL (trace level), Thermo Environment Instruments Inc., USA	0.05±0.025 ppb
O_3 concentration *(10 m)*	5 min	UV absorption	Model 49C Thermo Environment Instruments Inc., USA	1±0.5 ppb
Air temperature *(Met 1, 0.5 m and 5 m)*	1 min	Pt-100 Ω resistance sensor	MP-103A-CG030-W4W Rotronic, Switzerland	±0.1 K
Relative humidity *(Met 1, 0.5 m and 5 m)*	1 min	Capacitive sensor	MP-103A-CG030-W4W Rotronic, Switzerland	±1.5%
Surface wetness *(Met 1)*	1 min	Surface wetness grids at soil surface	237 WSG, Campbell Scientific Ltd., UK	–
Global radiation flux *(Met 1, 5 m)*	1 min	Pyranometer sensor	LI200SZ (LI-COR, Lincoln, Nebraska, USA)	< ±3%
Eddy covariance; three dimensional wind and temperature fluctuations *(Met 2, 4 m)*	10 Hz	3-D ultrasonic anemometer	Solent 1012R2, Gill Instruments, UK	±1.5%
H_2O mixing ratio *(Met 2, 4 m)*	10 Hz	Infrared closed-path absorption	IRGA LI-COR 6262 (LI-COR, Lincoln, Nebraska, USA)	±1%
Shortwave radiation in and out *(Met 2, 8.5 m)*	1 min	Pyranometer sensor	Kipp & Zonen Pyranometer CM 21	±2%
Longwave radiation in and out *(Met 2, 8.5 m)*	1 min	Pyranometer sensor	Kipp & Zonen Pyrgeometer CG	±3%

[1] 20 min: dry season (12–13 September), 40 min: transition period (7–31 October), 60 min: wet season (1–14 November)

[2] IC: ion chromatography, FIA: flow injection analysis

Table 2. Summary of trace gas and aerosol mixing ratios[*] during the dry season (12–13 September), the transition period (7–31 October) and the wet season (1–14 November) at FNS during LBA-SMOCC 2002.

	Dry season				Transition period				Wet season			
Species	m (ppb)	P 0.25 (ppb)	P 0.75 (ppb)	n (1)	m (ppb)	P 0.25 (ppb)	P 0.75 (ppb)	n (1)	m (ppb)	P 0.25 (ppb)	P 0.75 (ppb)	n (1)
NO	0.09	0.07	0.15	372	0.09	0.07	0.17	295	0.12	0.07	0.13	229
NO_2	4.54	2.85	6.46	630	1.78	1.23	2.56	697	1.07	0.82	1.76	268
O_3	24.3	11.76	34.87	826	25.59	15.91	32.95	781	14.74	10.77	19.39	316
NH_3	1.81	1.10	2.91	298	1.06	0.5	1.74	236	0.55	0.38	0.85	60
HNO_3	0.16	0.10	0.25	317	0.06	0.03	0.13	210	0.06	0.04	0.08	52
HONO	0.12	0.08	0.27	323	0.07	0.05	0.09	315	0.06	0.04	0.07	139
Aerosol NH_4^+	1.01	0.73	1.51	291	0.54	0.33	0.85	267	0.47	0.32	0.62	66
Aerosol NO_3^-	0.34	0.17	0.61	297	0.09	0.06	0.15	282	0.06	0.04	0.07	33

[*] m: median, P 0.25: 0.25 percentile, P 0.75: 0.75 percentile, n: number of determined data points above the limit of detection (for aerosol species PM 2.5 and bulk measurements were included). NO_x/O_3 data were synchronized to the WAD/SJAC data, i.e. one data point is available for each gas and each aerosol measurement of the WAD/SJAC).

Title Page

Abstract | Introduction

Conclusions | References

Tables | Figures

◀◀ | ▶▶

◀ | ▶

Back | Close

Full Screen / Esc

Print Version

Interactive Discussion

EGU

Table 3. Ranges of surface resistances R_c for HNO_3 and HONO for daytime and nighttime used to estimate flux scenarios at FNS during LBA-SMOCC 2002.

	Scenario	$R_c(HNO_3)$ $[s\,m^{-1}]$	$R_c(HONO)$ $[s\,m^{-1}]$
Day	high	1	50
	low	50	200
Night	high	1	15
	low	15	100
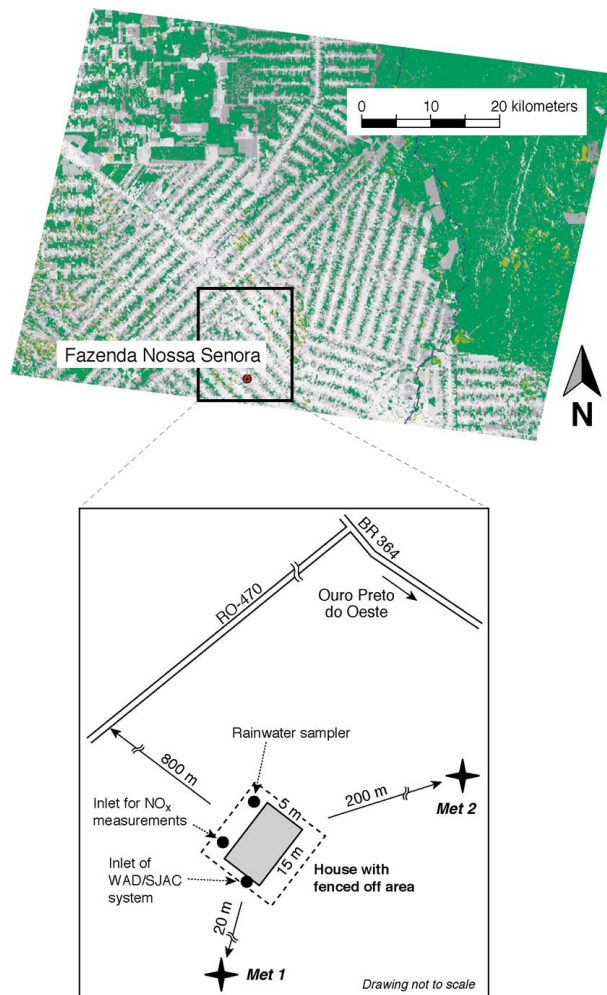
Fig. 1. Location of the LBA-SMOCC measurement site "Fazenda Nossa Senhora Aparecida" (FNS) in Rondonia, Brazil.

EGU
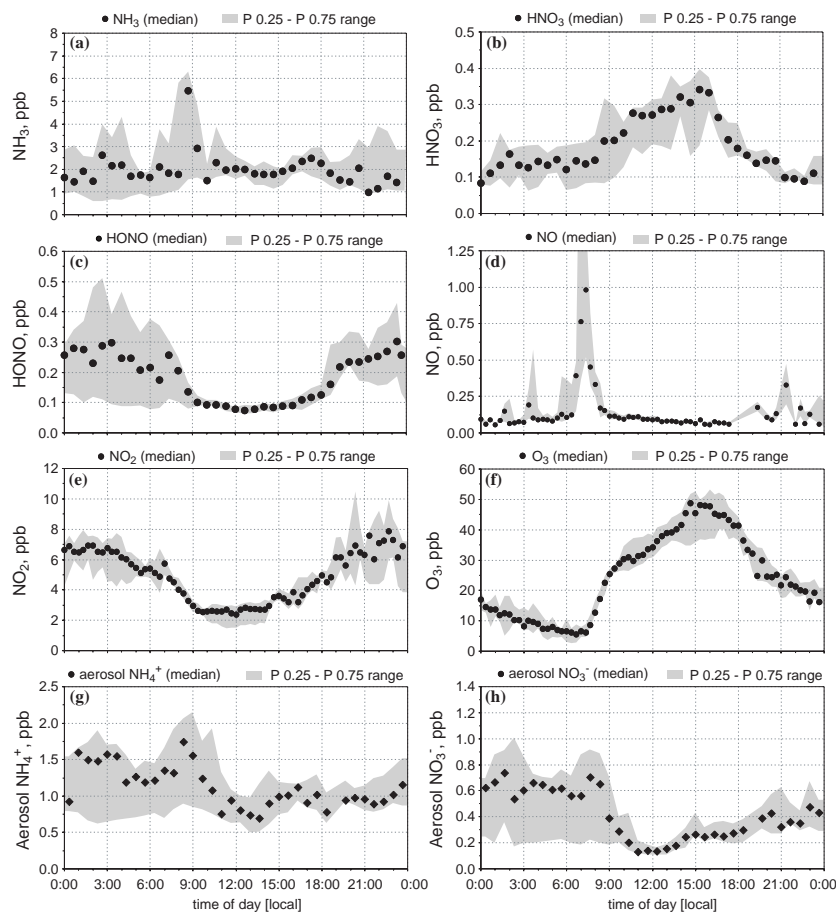
Fig. 2. Diel variations of **(a)** NH_3, **(b)** HNO_3, **(c)** HONO, **(d)** NO, **(e)** NO_2, **(f)** O_3, **(g)** aerosol NH_4^+ (PM 2.5) and **(h)** aerosol NO_3^- (PM 2.5) measured during 12–23 September 2002 (dry season, biomass burning) at FNS during LBA-SMOCC 2002. Symbols and grey shading represent medians and interquartile ranges (0.25 to 0.75 percentiles), respectively.

Title Page

Abstract | Introduction

Conclusions | References

Tables | Figures

◄ | ►|

◄ | ►

Back | Close

Full Screen / Esc

Print Version

Interactive Discussion

EGU
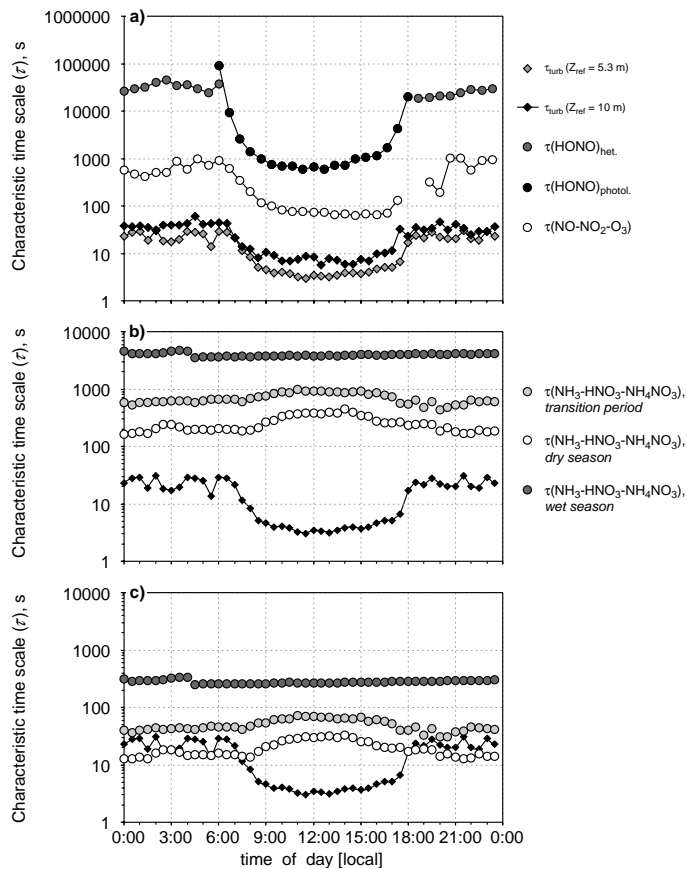
Fig. 3. Diel variation of characteristic turbulent time scale τ_{turb} for the reference heights z_{ref} =10 m and z_{ref}=5.3 m in comparison to **(a)** chemical time scale of the NO-NO$_2$-O$_3$ triad (τ(NO-NO$_2$ – O_3)), daytime HONO photolysis (τ(HOHO)$_{photol.}$) and heterogeneous HONO formation at night (τ(HOHO)$_{het.}$, dry season only), **(b)** upper estimate of equilibration time scales for the NH$_3$/HNO$_3$/NH$_4$NO$_3$ system τ(NH$_3$-NO$_3$-NH$_4$NO$_3$) (α=0.1, PM$_{inorg.}$ ≤20%) and **(c)** lower estimate of τ(NH$_3$-NO$_3$-NH$_4$NO$_3$) (α=1, PM$_{soluble}$ ≤60%) at FNS during LBA-SMOCC 2002. Except for τ(HOHO)$_{het}$, data from all seasons were used.

EGU
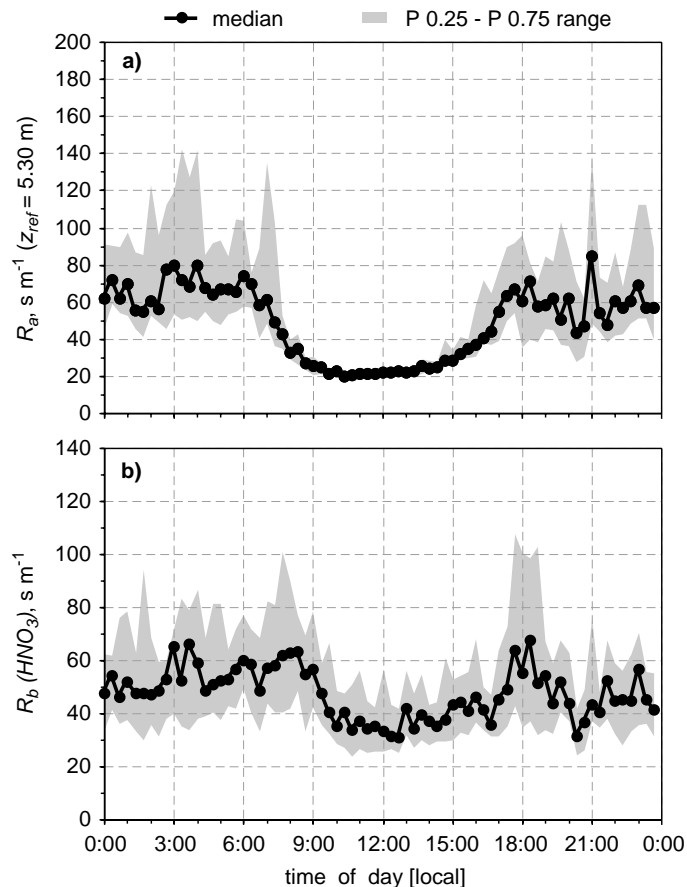
Fig. 4. Diel variations of **(a)** turbulent resistance (R_a) and **(b)** quasi-laminar boundary layer resistance (R_b) exemplary for HNO_3 at FNS during LBA-SMOCC 2002. Symbols and grey shading represent medians and interquartile ranges (0.25 to 0.75 percentiles), respectively. Data from all seasons were used.

EGU
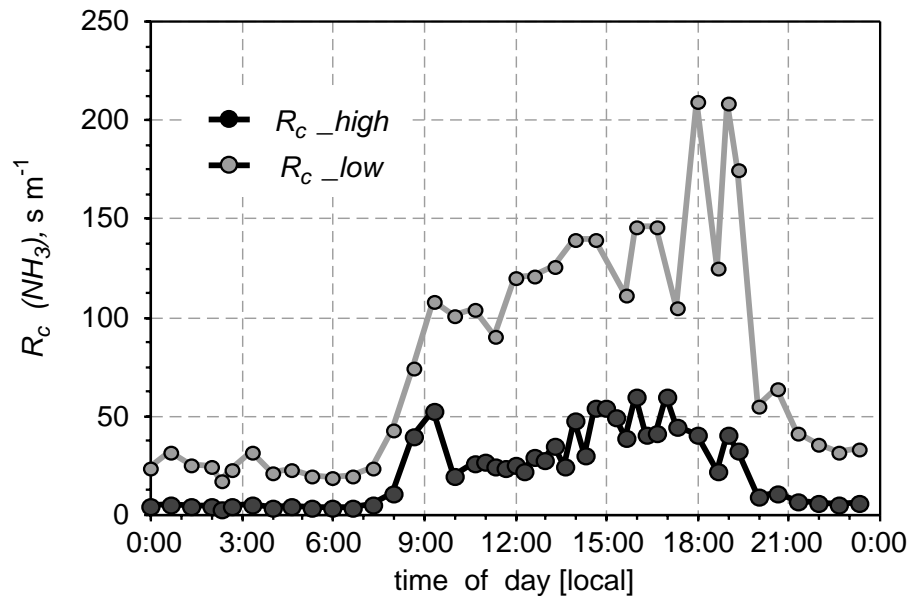
Fig. 5. Median diel variation of the estimated lower (low) and upper (high) bulk surface resistance $R_c(NH_3)$ (sum of the parallel resistances $R_s(NH_3)$ and $R_d(NH_3)$) at FNS during LBA-SMOCC 2002. Data from all seasons were used.
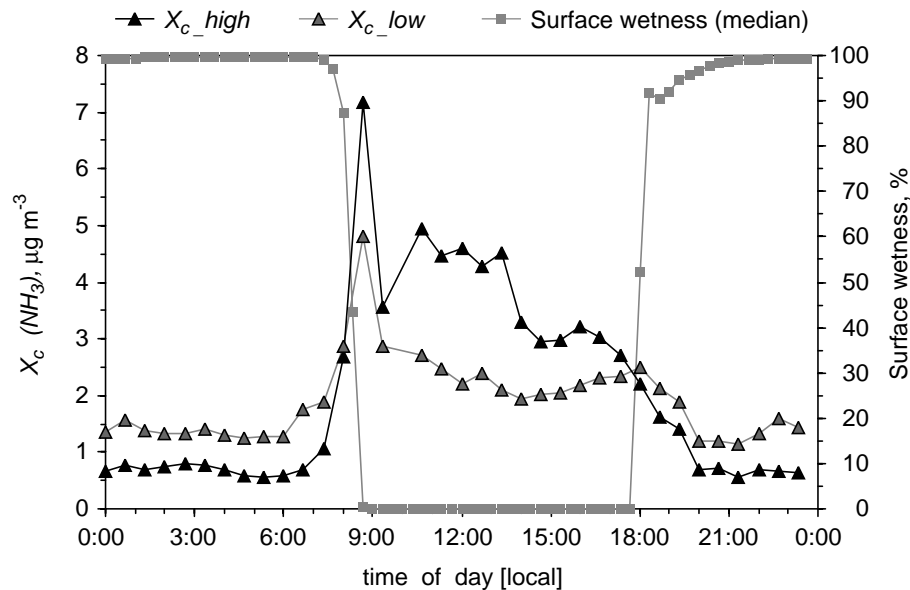
Fig. 6. Median diel variation of the simulated lower (low) and upper (high) NH_3 canopy compensation point $X_c(NH_3)$, and the median diel variation of the measured surface wetness, shown exemplarily for a period during the dry season (12–23 September) at FNS during LBA-SMOCC 2002. For details about low and high estimates, see text.

EGU
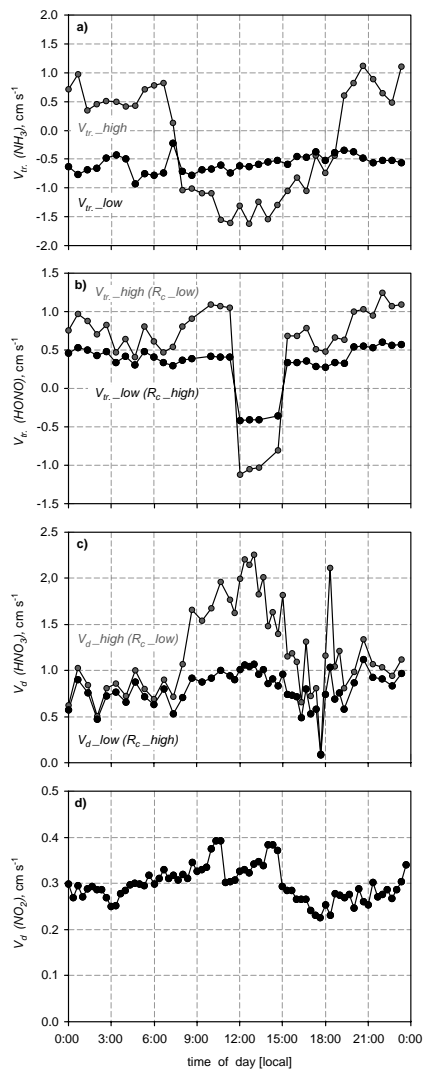
Fig. 7. Median diel variation of simulated lower (low) and upper (high) transfer velocity $V_{tr.}$ for bi-directional surface atmosphere exchange of **(a)** NH_3, **(b)** HONO, and deposition velocity V_d for **(c)** HNO_3 and **(d)** NO_2 at FNS during LBA-SMOCC 2002. Data from all seasons were used, except for $V_{tr.}$(HONO), which only represents results from the dry season, since negligible small upward HONO fluxes were predicted during transition period and wet season.

EGU
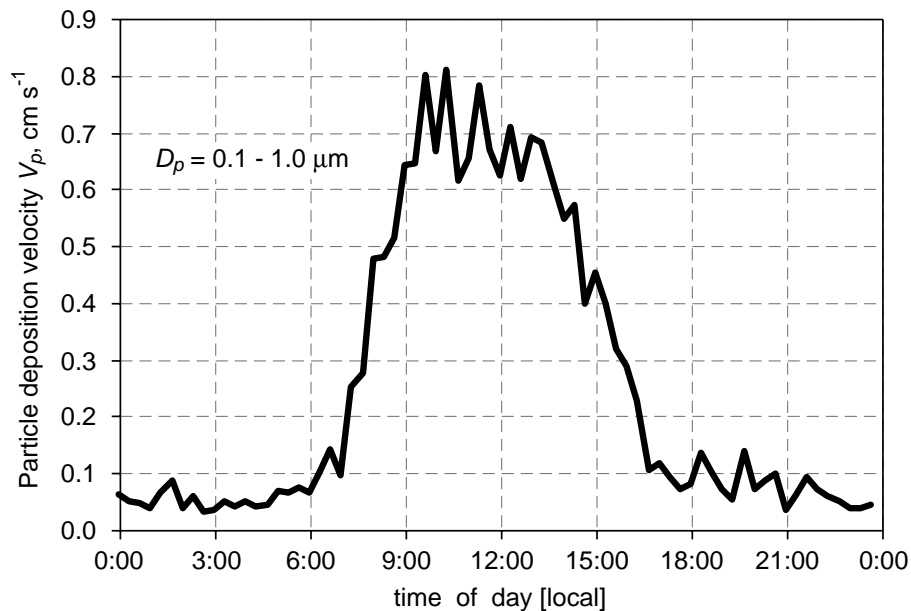
Fig. 8. Median diel course of the particle deposition velocity V_p using the empirical parameterization derived by Wesely et al. (1985) for aerosol particles with D_p=0.1–1 μm at FNS during LBA-SMOCC 2002.
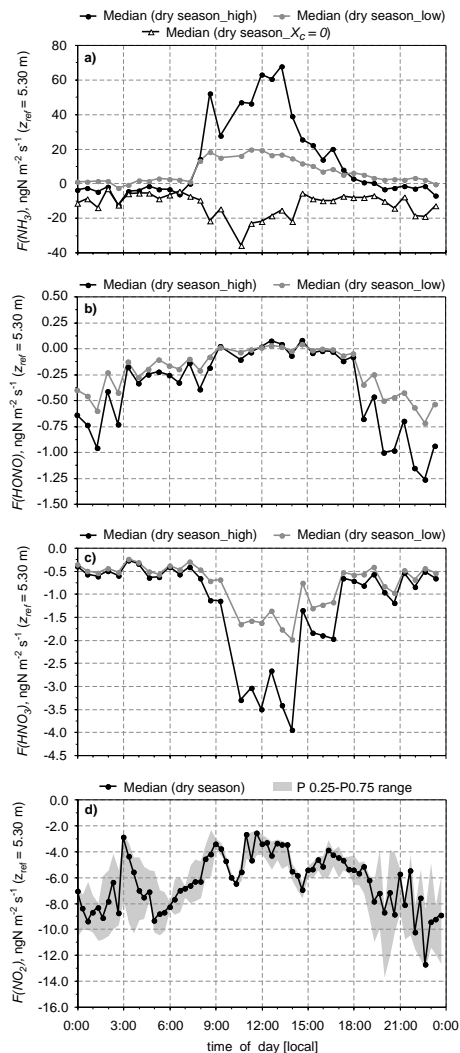
Fig. 9. Median diel courses of estimated lower (low) and upper (high) surface-atmosphere trace gas exchange fluxes for: **(a)** NH$_3$, **(b)** HONO and **(c)** HNO$_3$. Bi-directional NH$_3$ flux scenarios were complemented by a net deposition scenario (X$_c$(NH$_3$)=0). The median flux of **(d)** NO$_2$ is estimated using R_c values from Kirkman et al. (2002) and is presented with interquartile ranges (0.25 to 0.75 percentiles). Medians have been calculated exemplarily for a period during the dry season (12–23 September) at FNS during LBA-SMOCC 2002.
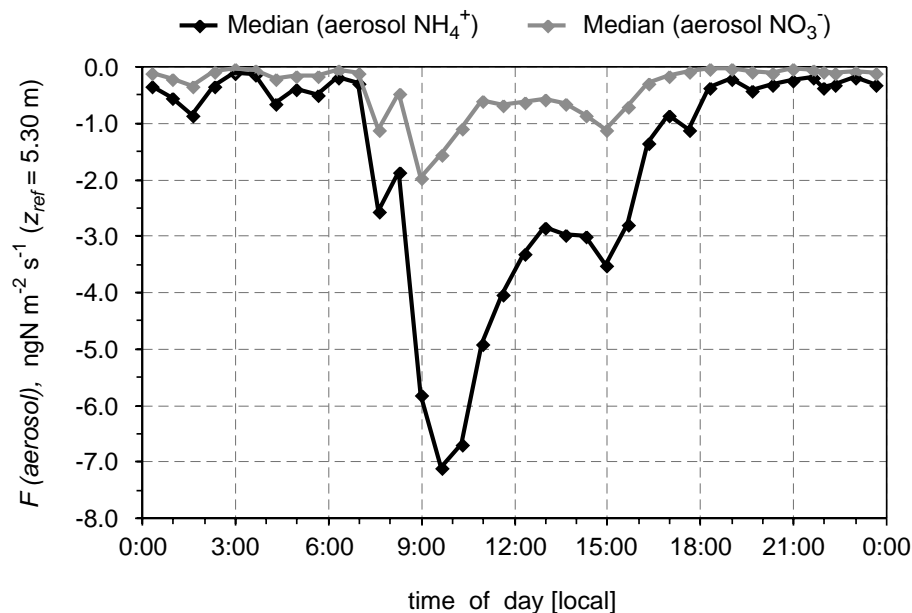
Fig. 10. Median diel courses of inferred deposition fluxes of aerosol NH_4^+ and aerosol NO_3^- shown exemplarily for a period during the dry season (12–23 September) at FNS during LBA-SMOCC 2002.

EGU
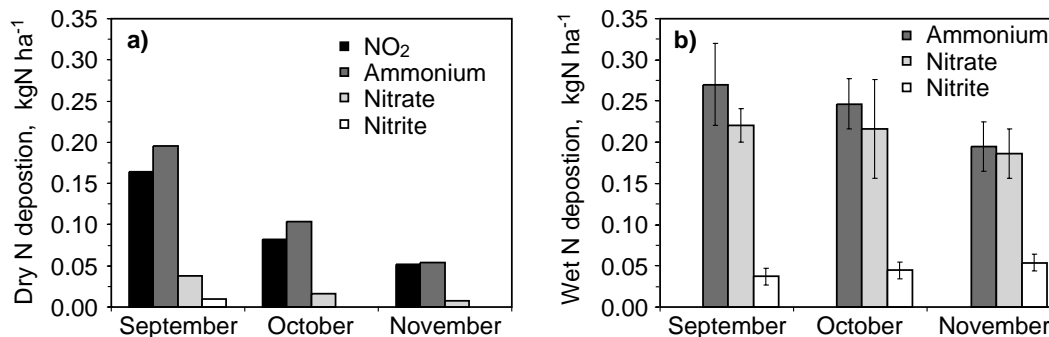
Fig. 11. Monthly estimates of **(a)** dry N deposition of NO_2, total ammonium (aerosol NH_4^+ + NH_3), total nitrate (aerosol NO_3^- + HNO_3) and nitrite (HONO) (averages of lower and upper estimates are shown, except for NH_3 which represents an average of all three estimates (cf. Fig. 9a) and **(b)** wet N deposition of ammonium, nitrate and nitrite (error bars represent measurement uncertainties) for September (dry season, biomass burning), October (transition period) and November (wet season, clean conditions) at FNS during LBA-SMOCC 2002.
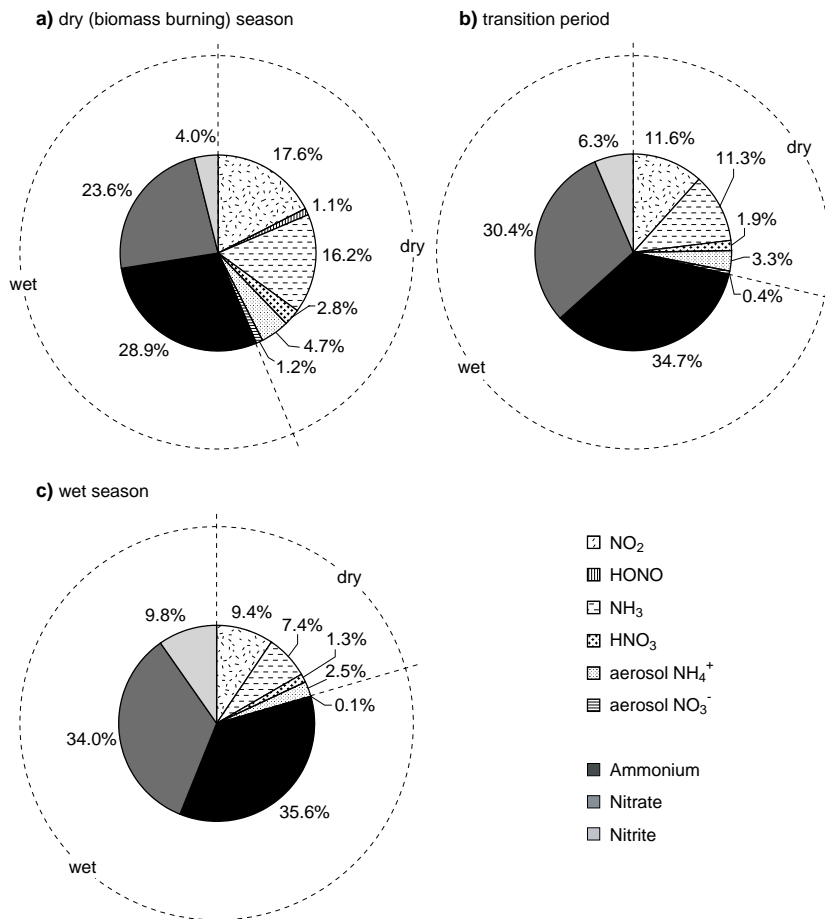
Fig. 12. Contribution of inorganic N compounds to the estimated total N deposition for **(a)** September (dry season, biomass burning), **(b)** October (transition period) and **(c)** November (wet season, clean conditions) at FNS during LBA-SMOCC 2002. Dry deposition of gaseous species is presented using averages of lower and upper estimates.
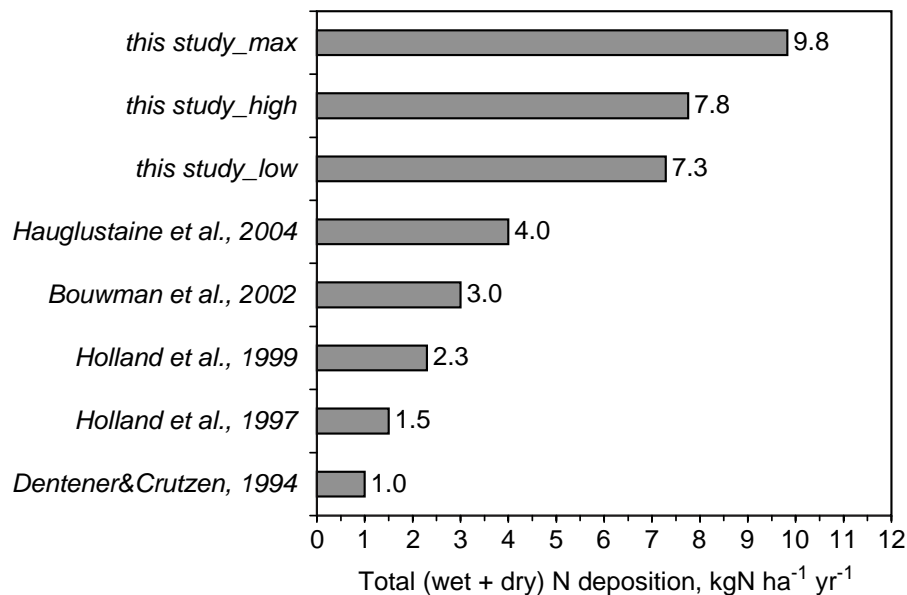
EGU

Fig. 13. Comparison of the annual (dry + wet) N deposition predicted by global chemistry and transport models for the Amazon region with the annual (dry + wet) N deposition estimated in this study. "This study_low" and "this study_high" correspond to lower and upper flux estimates. "This study_max" corresponds to the upper flux estimate, but considering NH_3 to be net deposited ($X_c(NH_3)$=0, cf. Fig. 9a).